


RESEARCH ARTICLE

B cells support the repair of injured tissues by adopting MyD88-dependent regulatory functions and phenotype

Ruxandra F. Sirbulescu¹  | Akshay Mamidi^{1,2} | Shu-Yi Claire Chan¹ | Gina Jin^{1,3} | Myriam Boukhali⁴ | Don Sobell¹ | Iulian Ilies⁵ | Joon Yong Chung³ | Wilhelm Haas⁴ | Michael J. Whalen³ | Ann E. Sluder¹ | Mark C. Poznansky¹

¹Vaccine and Immunotherapy Center, Department of Medicine, Massachusetts General Hospital, Harvard Medical School, Boston, Massachusetts, USA

²School of Chemical and Biochemical Engineering, Nanyang Technological University, Singapore, Singapore

³Neuroscience Center, Department of Pediatrics, Massachusetts General Hospital, Harvard Medical School, Boston, Massachusetts, USA

⁴Center for Cancer Research, Department of Medicine, Massachusetts General Hospital, Harvard Medical School, Boston, Massachusetts, USA

⁵Healthcare Systems Engineering Institute, Department of Mechanical and Industrial Engineering, Northeastern University, Boston, Massachusetts, USA

Correspondence

Ruxandra F. Sirbulescu and Mark C. Poznansky, Vaccine and Immunotherapy Center, 149 13th Street, Charlestown, MA 02129, USA. Email: rsirbulescu@mgh.harvard.edu and mpoznansky@mgh.harvard.edu

Funding information

HHS | NIH | National Institute of Neurological Disorders and Stroke (NINDS), Grant/Award Number: R01NS117598; Vaccine and Immunotherapy Center Innovation Fund; Holy Cross Hospital, Ft. Lauderdale, FL

Abstract

Exogenously applied mature naïve B220⁺/CD19⁺/IgM⁺/IgD⁺ B cells are strongly protective in the context of tissue injury. However, the mechanisms by which B cells detect tissue injury and aid repair remain elusive. Here, we show in distinct models of skin and brain injury that MyD88-dependent toll-like receptor (TLR) signaling through TLR2/6 and TLR4 is essential for the protective benefit of B cells in vivo, while B cell-specific deletion of MyD88 abrogated this effect. The B cell response to injury was multi-modal with simultaneous production of both regulatory cytokines, such as IL-10, IL-35, and transforming growth factor beta (TGFβ), and inflammatory cytokines, such as tumor necrosis factor alpha (TNFα), IL-6, and interferon gamma. Cytometry analysis showed that this response was time and environment-dependent in vivo, with 20%–30% of applied B cells adopting an immune modulatory phenotype with high co-expression of anti- and pro-inflammatory cytokines after 18–48 h at the injury site. B cell treatment reduced the expression of TNFα and increased IL-10 and TGFβ in infiltrating immune cells and fibroblasts at the injury site. Proteomic analysis further showed that B cells have a complex time-dependent homeostatic effect on the injured microenvironment, reducing the expression of inflammation-associated proteins, and increasing proteins associated

Abbreviations: CCI, controlled cortical impact; CD, cluster of differentiation; CNS, central nervous system; DAMP, damage-associated molecular pattern; ECM, extracellular matrix; GO, gene ontology; HA, hyaluronic acid; HMGB1, high-mobility group protein B1; HSP60, heat-shock protein 60; IFNγ, interferon gamma; Ig, immunoglobulin; IL, interleukin; LC-MS, liquid chromatography mass spectrometry; LPS, lipopolysaccharide; MALP-2, macrophage-activating lipopeptide-2; MS3, triple-stage mass spectrometry; MWM, Morris water maze; MyD88, myeloid differentiation primary response 88 protein; NORT, novel object recognition test; Pam3CSK4, Pam3CysSerLys4: synthetic bacterial tripalmitoylated lipopeptide; PAMP, pathogen-associated molecular pattern; PCA, principal component analysis; TBI, traumatic brain injury; TGFβ, transforming growth factor beta; TLR, toll-like receptor; TMT, tandem mass tag; TNFα, tumor necrosis factor alpha; WT, wild-type.

with proliferation, tissue remodeling, and protection from oxidative stress. These findings chart and validate a first mechanistic understanding of the effects of B cells as an immunomodulatory cell therapy in the context of tissue injury.

KEYWORDS

B cells, immunomodulation, injury, MyD88, regulatory mechanisms, TLR

1 | INTRODUCTION

Beyond their classical role in the production of antibodies, B cells have been increasingly recognized in recent years as important regulators of the immune response that can control host defense against pathogens and protect from aberrant autoimmune reactions.¹ While these roles have been described in endogenous B cell populations, only a few studies to date have examined the potential of using locally delivered B cells as a cell-based therapeutic agent to modulate immune responses in the context of tissue injury. In a first study of its kind, B cells purified from the bone marrow were shown to support functional cardiac recovery significantly better than stem cells in a rat model of myocardial infarction.² We have recently shown that exogenous mature naïve B220⁺/CD19⁺/IgM⁺/IgD⁺ B cells can be applied therapeutically to injured tissues to successfully restore function and promote repair in diverse model systems, including diabetic skin wound healing,³ and contusion traumatic brain injury (TBI).⁴ When applied to full-thickness skin wounds, B cells, but not T cells, significantly accelerated wound closure by 2–3 days in wild-type (WT) mice and by 5–6 days in obese diabetic mice, and remarkably also enhanced the ingrowth of blood vessels and peripheral nerves.³ In a mouse model of contusion TBI a single administration of B cells, but not T cells, delivered into the brain parenchyma at the time of injury, led to significantly reduced deficits in learning and memory tasks as well as lesion volume at 35 days post-injury, and mitigated gliosis and microglial activation.⁴ Independently, in an experimental model of stroke, intravenous infusion of IL-10-producing B cells was observed to reduce inflammation and infarct volume.^{5,6} Collectively, these studies suggest that B cells applied in the context of injury actively modulate the local microenvironment and support tissue repair.

The molecular pathways that underlie the B cell response after direct application into an injured or inflamed tissue are not well understood. The present study investigates which molecular cues in the injured microenvironment may activate the introduced B cells, how the B cells respond phenotypically and functionally to these cues, and cellular and molecular changes in the injured microenvironment that are associated with the therapeutic

introduction of B cells. We provide a first mechanistic view of the B cell response at a site of tissue injury, and demonstrate that the molecular response of B cells is highly complex, involving multiple immunomodulatory cytokines. Using a cutaneous injury model, we show that B cell application significantly reduced expression of proteins associated with inflammation, apoptosis, and oxidative stress, and increased expression of factors associated with cell proliferation, cell growth, oxidative stress protection, and control of inflammation. B cells applied to the wound adopted a distinct time-dependent regulatory phenotype, producing expected immunoregulatory cytokines IL-10, IL-35, and TGF β , but also IL-2, IL-4, IL-6, and TNF α , that subsequently altered the secretome of neighboring infiltrating macrophages and neutrophils. Using two distinct model systems, a full-thickness cutaneous excision lesion and contusion TBI, we further found that MyD88-dependent Toll-like receptor (TLR) signaling plays an essential role in environmental sensing by B cells, since B cell-specific MyD88 knockout completely abrogated the protective benefit of exogenous B cells. Regulatory cytokines IL-10, and to a lesser extent IL-35, have important, but not exclusive effector functions. In vitro stimulation experiments further confirmed that specific activation of B cells with TLR 2, TLR 4, and TLR 6 agonists of either bacterial or cellular origin can induce a response similar to that observed following in vivo exposure to injured tissues. We term this newly identified response of mature naïve B cells upon direct introduction into an injured microenvironment, *pligodraxis*, from the Greek *pligí* = wound, and *drási* = action, indicating the specific activation of B cells in the microenvironment of injured tissues to drive a multi-modal immunomodulatory and pro-regenerative response.

2 | MATERIALS AND METHODS

2.1 | Animals

Studies were conducted in 8–12-week-old male wild-type C57Bl6/J mice (Jackson Laboratories). Male C57Bl6/J (WT), B6.SJL-Ptprc^aPepc^b/BoyJ (CD45.1⁺), B6.129P2-Il10^{tm1Cgn}/J (IL-10^{-/-}), B6.129P2(SJL)-Myd88^{tm1.1Defr}/J

(MyD88^{-/-}), B6.129S1-II12a^{tm1Jm/J} (IL-35^{-/-}), and B6.129S-Tnf^{tm1Gkl/J} (TNF α ^{-/-}) were used as isogenic donors for B cell isolation. Animals were maintained under standard laboratory care conditions, at temperatures ranging between 20 and 23°C, under a 12:12 h light:dark cycle, with ad libitum access to food and acidified water. All animal procedures were performed following the Public Health Service Policy on Humane Care of Laboratory Animals and approved by the Institutional Animal Care and Use Committee of Massachusetts General Hospital. All efforts were made to reduce the number of animals used and to minimize animal suffering.

2.2 | Cell isolation

Mouse spleens were collected in ice cold EasySepTM buffer (STEMCELL Technologies) containing 2% fetal bovine serum (FBS) and 1 mM ethylenediaminetetraacetic acid (EDTA) in phosphate-buffered saline (PBS). Spleens were dissociated mechanically through a 40 μ m cell strainer and the splenocyte suspension was processed for negative B cell selection through immunomagnetic separation, using commercially available cell isolation kits (STEMCELL Technologies) according to the manufacturer's instructions. The purity of the B cell isolate was over 98% mature naïve CD45R+/CD19+ B lymphocytes, as validated by flow cytometry analysis.³

2.3 | Wound models and tissue sampling

2.3.1 | Wound healing studies

Full-thickness excisional wounds through the dorsal skin were induced as described previously.³ Briefly, mice were anesthetized and the dorsal skin was shaved and depilated. Analgesia was provided pre-operatively with 0.08 mg/kg buprenorphine injected subcutaneously. The dorsal skin was tented, and a 5-mm biopsy punch was passed through the skin fold, creating two symmetrical wounds on each side of the back. Each wound had an initial area of approximately 20 mm². Silicone splints with an inner diameter of 7 mm (Sigma-Aldrich) were attached around the wounds using Vetbond tissue adhesive (3M). Wounds were randomly allocated to treatment categories. Cell suspensions in PBS or equal volumes of PBS solution alone (saline control) were applied directly onto the wound bed using a manual pipette. The splinted wounds were then covered with TegadermTM transparent dressing (3M). For the wound healing studies, the mice were allowed to heal for 16 days, and high-resolution photographs of the wounds (0.018 mm/pixel) were collected every 2 days. To acquire

the images of the dorsal wounds, animals were briefly anesthetized using 3% isoflurane in oxygen. The area of remaining open wound, as well as the area of the visible scar at the end point of each study were assessed using ImageJ software (National Institutes of Health). The splint area in each image was used both to calibrate the measurements of the wound and to control for parallax error. Analysis of the wound areas was performed by experimenters blinded to the treatment conditions.

2.3.2 | Cell retrieval studies

For the analysis of cellular responses to B cell application in the wound microenvironment, four full-thickness excision lesions were generated in the dorsal skin as described above (see Figure 4A) and 10–15 \times 10⁶ B cells in 20 μ l PBS were applied to each site before covering with adhesive dressing. Each mouse also received two localized subcutaneous injections under intact posterior dorsal skin with equal doses of B cells or saline. After defined time intervals, 18 h, 2, 4, or 10 days, the mice were lightly anesthetized using 3% isoflurane in O₂, and 10–20 μ l of a working solution of brefeldin A (GolgiPlugTM, BD Pharmingen) in PBS was applied to each of the treated wound and subcutaneous sites to allow the accumulation of cytokines within cells. After 4 h of incubation, the mice were euthanized and tissue biopsies including the wounds and the subcutaneous injection sites were collected. Tissue biopsies were enzymatically dissociated for 30 min at 37°C with gentle rocking in RPMI medium containing 5% FBS, 0.5% L-glutamine, 0.5% penicillin-streptomycin, 1.5 mg/ml, 0.25 U/mg Collagenase D (Roche), 1.5 mg/ml, 400 U/mg hyaluronidase from bovine testes (Millipore Sigma), 0.4 mg/ml, 400 U/mg DNase I (Roche), 0.025 mg/ml, and 10 U/mg Dispase I (Millipore Sigma). Tissues were then mechanically minced into smaller pieces, followed by further enzymatic dissociation for another 30 min in the same solution at 37°C with gentle rocking. The digested tissues from individual wound and subcutaneous samples were then pooled for each mouse and passed through a 100 μ m cell strainer followed by a 40 μ m cell strainer, resulting in single-cell suspensions.

2.4 | Controlled cortical impact (CCI)

All surgical procedures, including the injury and the application of cells or saline, were performed by an experimenter blinded to the treatment conditions, who did not take part in the preparation of treatment doses for injection. Mice were anesthetized with 4% isoflurane (Baxter) for 90 s in a mixture of 70% N₂O and 30% O₂ using a

Fluotec3 vaporizer (Colonial Medical) and placed in a stereotaxic frame. Anesthesia was maintained with 3% isoflurane. After a medial incision in the scalp, a craniotomy was made using a portable drill and 5-mm trephine over the left parieto-temporal cortex, and the bone flap was discarded. An ipsilateral intraparenchymal injection was delivered at approximately -1 mm from bregma on the anterior/posterior axis, $+2$ mm medial/lateral, at a depth of 3 mm through the left parietal cortex. A total of $5 \mu\text{l}$ of saline solution containing either 2×10^6 WT B cells, $\text{IL-10}^{-/-}$ B cells, $\text{MyD88}^{-/-}$ B cells, or saline control alone, was injected using a $10\text{-}\mu\text{l}$ Hamilton syringe with a 26 s gauge blunt tip needle (Hamilton Company). Mice were randomly allocated to the selected treatment condition. The selected cell dose has been optimized previously as described.⁴ Cell application was performed immediately before CCI to ensure correct and consistent injection of cells while the brain structure was intact. Mice were immediately thereafter subjected to CCI using a pneumatic cylinder with a 3-mm flat-tip impounder, at a velocity of 6 m/s, a depth of 0.6 mm, and a 100-ms impact duration. The craniotomy was left open and the skin was closed over the skull using 6–0 nylon sutures (Fisher Scientific, Waltham, MA).

2.5 | Proteomics

2.5.1 | Tissue sampling

Full-thickness excision wounds were generated in the dorsal skin of mice as described above. The wounds were treated either with a purified B cells at 1.5×10^6 cells suspended in $20 \mu\text{l}$ saline, or with saline control. After defined time intervals, 0 days (approximately 10 min) ($n = 4$ per treatment), 1 day ($n = 4$ per treatment), 4 days ($n = 5$ per treatment), and 10 days ($n = 3$ per treatment), the mice were euthanized, and the wound area, including wound margin and subcutaneous layers was excised and flash-frozen in liquid nitrogen, then stored at -80°C until lysis.

2.5.2 | Multiplexed quantitative proteomics

Tissue samples were homogenized and lysed as described⁷ using a bead mill, zirconium oxide beads (1 mm, Next Advance), and a lysis buffer of 75 mM NaCl, 3% SDS, 1 mM NaF, 1 mM beta-glycerophosphate, 1 mM sodium orthovanadate, 10 mM sodium pyrophosphate, 1 mM PMSF and $1\times$ Roche Complete Mini EDTA free protease inhibitors in 50 mM HEPES, pH 8.5. Lysates were then sonicated for 5 min in a sonicating water bath before cellular debris was pelleted by centrifugation at 14,000 rpm for 5 min.

Proteins were reduced with DTT and alkylated with iodoacetamide as previously described and precipitated via methanol-chloroform precipitation.⁸ Precipitated proteins were reconstituted in $300 \mu\text{l}$ of 1 M urea in 50 mM HEPES, pH 8.5 and digested in a two-step process starting with overnight digest at room temperature with Lys-C (Wako) followed by six hours of digestion with trypsin (sequencing grade, Promega) at 37°C . The digest was acidified with TFA and peptides were desalted with C_{18} solid-phase extraction (SPE) (Sep-Pak, Waters) as previously described.⁸ The concentration of the desalted peptide solutions was measured with a BCA assay, and peptides were aliquoted into $50 \mu\text{g}$ portions, which were dried under vacuum and stored at -80°C until they were labeled with 10-plex TMT reagents (Thermo Scientific) as described previously.⁸ Pooled TMT-labeled samples were desalted via C_{18} SPE on Sep-Pak cartridges as described above and subjected to basic pH reversed-phase liquid chromatography (bRPLC)⁸ over a 4.6×250 mm ZORBAX Extend C_{18} column ($5 \mu\text{m}$, 80 \AA , Agilent Technologies) with concatenated fraction combining as previously described, and 12 fractions were subjected to quantitative proteomics analysis.

All liquid chromatography mass spectrometry (LC-MS2/MS3) experiments were conducted on an Orbitrap Fusion (Thermo Fisher Scientific) coupled to an Easy-nLC 1000 (Thermo Fisher Scientific) with chilled autosampler. Peptides were separated on an in-house pulled, in-house packed microcapillary column (inner diameter, $100 \mu\text{m}$; outer diameter, $360 \mu\text{m}$). Columns were packed to a final length of 30 cm with GP- C_{18} ($1.8 \mu\text{m}$, 120 \AA , Sepax Technologies). Peptides were eluted with a linear gradient from 11% to 30% ACN in 0.125% formic acid over 165 min at a flow rate of 300 nl/min, while the column was heated to 60°C . Electrospray ionization was achieved by applying 1500 V through a stainless-steel T-junction at the inlet of the microcapillary column.

The Orbitrap Fusion was operated in data-dependent mode, with a survey scan performed over an m/z range of 500–1,200 in the Orbitrap with a resolution of 6×10^4 , automatic gain control (AGC) of 5×10^5 , and a maximum injection time of 100 ms. The most abundant ions detected in the survey scan were subjected to MS2 and MS3 experiments to be acquired in a 5-s experimental cycle. For MS2 analysis, doubly charged ions were selected from an m/z range of 600–1200, and triply and quadruply charged ions from an m/z range of 500–1200. The ion intensity threshold was set to 5×10^5 and the isolation window to 0.5 m/z . Peptides were isolated using the quadrupole and fragmented using CID at 30% normalized collision energy at the rapid scan rate using an AGC target of 1×10^4 and a maximum ion injection time of 35 ms. MS3 analysis was performed using synchronous precursor selection (SPS).^{9,10} Up to 6 MS2 precursors were simultaneously

isolated and fragmented for MS3 analysis with an isolation window of 2.5 m/z and HCD fragmentation at 50% normalized collision energy. MS3 spectra were acquired at a resolution of 5×10^3 with an AGC target of 5×10^4 and a maximum ion injection time of 250 ms.

Data were processed using an in-house developed software suite.¹¹ MS2 data were annotated using the Sequest algorithm¹² to search the mouse Uniprot protein sequence databases (including known contaminants such as trypsin), and a target-decoy database strategy was applied to measure false-discovery rates of peptide and protein identifications. Searches were performed with a 50-ppm precursor mass tolerance; 10-plex TMT tags on lysine residues and peptide n-termini (+229.162932 Da) and carbamidomethylation of cysteines (+57.02146 Da) were set as static modifications and oxidation of methionine (+15.99492 Da) as a variable modification. Data were filtered to a peptide and protein false discovery rate of less than 1% using the target-decoy search strategy.¹³ Peptides that matched to more than one protein were assigned to that protein containing the largest number of matched redundant peptide sequences following the law of parsimony.¹¹ TMT reporter ion intensities were extracted from the MS3 spectra selecting the most intense ion within a 0.003 m/z window centered at the predicted m/z value for each reporter ion and spectra were used for quantification if the sum of the S/N values of all reporter ions was ≥ 300 and the isolation specificity for the precursor ion was ≥ 0.75 . Protein intensities were calculated by summing the TMT reporter ions for all peptides assigned to a protein. Intensities were first normalized based on the average intensity across all samples. In a second normalization step, protein intensities measured for each sample were normalized by the average of the median protein intensities measured across the samples. All mass spectrometer RAW files can be accessed through the MassIVE data repository (massive.ucsd.edu) under the accession number MSV000086632.

2.6 | Flow cytometry

To evaluate cell viability after retrieval from tissue digestion, the cell suspensions were washed and resuspended in PBS and stained using a Zombie UV fixable viability kit (Biolegend) for 30 min in the dark at 4°C with gentle rocking. The stained cells were then washed and resuspended in PBS containing 1% FBS, 0.01% sodium azide (RICCA Chemical) and 5% FcR blocking reagent (Miltenyi Biotec) for 10 min in the dark at 4°C. Blocked cells were then incubated for 30 min in the dark at 4°C with the following fluorophore-conjugated primary surface antibodies: Brilliant Violet 785-conjugated rat anti-mouse

CD19 (clone 6D5), Alexa Fluor® 700-conjugated rat anti-mouse/human CD45R/B220 (clone RA3-6B2), APC/Cy7-conjugated rat anti-mouse CD138 (clone 281-2) (all from Biolegend), Brilliant Ultraviolet 395-conjugated hamster anti-mouse CD69 (clone H1.2F3), PE-CF594-conjugated rat anti-mouse CD140a (clone APA5) (both from BD Biosciences, San Jose, CA). Surface-stained cells were washed and resuspended in fixation buffer (Biolegend) for 30 min at 4°C, followed by permeabilization wash buffer (1×) (Biolegend). Permeabilized cells were then incubated for 30 min in the dark at 4°C with the following fluorophore-conjugated primary intracellular antibodies: Brilliant Violet 421-conjugated mouse anti-mouse TGF- β 1 (clone TW7-16B4), Brilliant Violet 510-conjugated rat anti-mouse IFN- γ (clone XMG1.2), Brilliant Violet 605-conjugated rat anti-mouse IL-4 (clone 11B11), Brilliant Violet 711-conjugated rat anti-mouse TNF- α (clone MP6-XT22), PerCP/Cy5.5-conjugated rat anti-mouse IL-2 (clone JES6-5H4), PE/Cy7-conjugated rat anti-mouse IL-10 (clone JES5-16E3), APC-conjugated rat anti-mouse IL-6 (clone MP5-20F3) (all from Biolegend), fluorescein-conjugated rat anti-mouse IFN- β (clone RMMB-1), PE-conjugated rat anti-mouse IL-27/IL-35 EB13 Subunit (clone 355022) (both from R&D Systems). Cells were analyzed on an LSRFortessa X-20 flow cytometer (BD Biosciences) equipped with BD FACSDIVA™ software and 355, 405, 488, 561 and 640 nm lasers. At least 100,000 events were collected from each sample for analysis. Data were analyzed using the FlowJo software, version 10.3 (TreeStar, Inc.).

2.7 | Behavioral testing

The sequence of behavioral assessments is summarized in Figure S5. Testing was performed as described previously.⁴

2.7.1 | Wire grip test

Vestibulo-motor function was assessed using a wire grip test.¹⁴ Mice were placed on a 45-cm-long metal wire suspended 45 cm above the ground and allowed to traverse the wire for 60 s. The latency to fall within the 60 s interval was measured, and a wire grip score was quantitated using a 5-point scale. Testing was performed in triplicate and an average value calculated for each mouse on each test day.

2.7.2 | Rotarod

Mice were placed on an automated Rotarod apparatus (Harvard Apparatus) which accelerated from 4 to 40 r/min

over 60 s. Maximum trial duration was 300 s, or until the mouse fell off the rotarod. Each mouse was assessed three times per day with 5 min rest intervals. The average latency to drop and the average r/min speed attained over the three trials was recorded for each day of testing.

2.7.3 | Morris water maze (MWM)

The MWM was performed as previously described with minor modifications.¹⁵ Spatial learning was assessed at approximately the same time each day. Each mouse was subjected to seven hidden platform trials (1–2 trials per day) using a random set of starting positions at any one of the four quadrants. One trial consisted of the average latency from each of the four starting positions. In the first trial, if a mouse failed to find the platform within 90 s, then it was placed on the platform for ~10 s. Probe trials were performed 24 h after the last hidden platform trial by allowing the mice to swim in the tank for 30 s with the platform absent, and recording the time spent in the target quadrant.

2.7.4 | Porsolt forced swim test

Mice were placed in a cylindrical transparent glass tank of 30 cm (height) × 20 cm (diameter) filled with water at room temperature up to a height of 20 cm. A white Styrofoam box provided visual shielding on three sides. Mice were placed in the water for 6 min and swimming movements were recorded. Total active time (swimming, pawing/climbing the beaker wall) versus inactive time (passive flotation) was quantified for the last four minutes of the test.

2.7.5 | Y-maze spontaneous alternation test

The Y maze test was conducted in an apparatus constructed of white opaque acrylic, consisting of three 40-cm long arms joined at 120° angles, with a wall height of 15 cm. Each arm was labeled with a different contrasting visual cue (black-on-white square, circle, star). Mice were placed in the center of the apparatus and allowed to explore the maze for 10 min. Their movements were recorded using a webcam positioned directly overhead and Photo Booth software (ANY-maze). Normal exploratory behavior in rodents involves a preference to enter a less recently visited arm of the maze (spontaneous alternation). An alternation score was calculated by dividing the number of three successive choices that included one instance of each arm by the total number of arm entries (i.e.,

opportunities for alternation). The apparatus was cleaned with 10% ethanol between trials.

2.7.6 | Elevated plus maze

The apparatus consisted of two 130 × 8 cm platforms with an 8 × 8 cm square area at their intersection, elevated at 60 cm above ground. The closed arms of the platform had 10 cm walls, whereas the open arms had none. Each mouse was placed in the central area of the maze and video-recorded for 5 min. The apparatus was cleaned with 10% ethanol between trials. Video recordings were analyzed by ANY-Maze (Stoelting Co.) software for mean speed and percent time in closed and open arms.

2.7.7 | Novel object recognition test (NORT)

For the familiarization session, mice were placed in an open-field test apparatus (33 × 33 × 20 cm) and exposed to two identical objects for 10 min. In the test session, administered the next day, mice were exposed to a familiar object from the previous session and a novel object for 5 min. Video recordings were analyzed by ANY-Maze (Stoelting Co.). The discrimination index was calculated as the ratio between the time spent exploring familiar and novel objects during the test session. No habituation session was performed prior to the administration of the test.

2.8 | Histology

2.8.1 | Wound biopsies

Wound biopsies at the end point of the wound healing time course were collected using a 10-mm biopsy punch and fixed in 4% paraformaldehyde in PBS for 24–48 h at 4°C, after which the samples were dehydrated through graded ethanol and xylene washes and embedded in paraffin. Transverse sections through the wound bed were cut at a thickness of 5 μm and mounted onto microscopy slides. Serial sections were stained with hematoxylin and eosin (H&E) for evaluating neutrophil infiltration and with Masson's trichrome stain for visualizing collagen fibers. Stained slides were digitized at a resolution of 0.5 μm/pixel using an Aperio ScanScope XT brightfield scanner (Leica Biosystems). Digitized slides were used for scoring of tissue regeneration and neutrophil infiltration by observers blinded to the treatment conditions. For neutrophil infiltrate evaluation a minimum area of 3,500 μm² was examined in each wound.

2.8.2 | Brain samples

At 35 days after CCI and treatment, the mice were deeply anesthetized with ketamine (100 mg/kg) and xylazine (10 mg/kg), perfused transcardially with 10–15 ml of heparinized PBS to remove blood, and decapitated. The brains were rapidly extracted on ice, frozen in liquid nitrogen vapor, and stored at -80°C . For cryosectioning, the brains were embedded in M-1 embedding matrix (Thermo Fisher Scientific, Waltham, MA), and sectioned coronally at a thickness of $16\ \mu\text{m}$ using a cryostat. Sections were collected at $500\ \mu\text{m}$ intervals along the rostro-caudal axis, and thaw-mounted onto SuperFrost Plus Gold slides (Fisher Scientific, Waltham, MA).

2.9 | Histological evaluation

2.9.1 | Wound scoring

Sections stained with Masson's trichrome were scored as previously described.³ Individual measurements included: the amount of residual granulation tissue (scale: 1–4, from 1 = abundant to 4 = absent), collagen fiber orientation (scale: 1–3, from 1 = vertical fascicles to 3 = horizontal), maturity of collagen (scale: 1–3, from 1 = mostly new, light staining to 3 = mostly mature, dark staining comparable to intact), pattern of collagen deposition (scale: 1–3, from 1 = dense fascicles to 3 = reticular), angiogenesis (scale: 1–4, from 1 = absent to 4 = >3 capillaries/ $100\ \mu\text{m}^2$), thickness of scar tissue (scale: 1–3, from 1 = thin, $<400\ \mu\text{m}$ to 3 = thick, $>1000\ \mu\text{m}$), width of scar (scale: 1–3, from 1 = wide, $>1000\ \mu\text{m}$ to 3 = narrow, $<600\ \mu\text{m}$), and presence of newly growing cutaneous nerves (scale: 0–1, with 0 = absent and 1 = present). Scoring was performed on digitized slides by an experimenter blinded to the treatment conditions.

2.9.2 | Brain lesion volume measurement after TBI

Sections were stained with hematoxylin and high-resolution overview photographs of the slides were collected. Morphometric image analysis in ImageJ (NIH, Bethesda, MD) was used to determine the area of each hemisphere. For each section, the area of the injured hemisphere was subtracted from the area of the uninjured hemisphere and the difference was multiplied by 0.5 to obtain the volume of brain tissue loss, expressed in mm^3 . All samples were coded, and measurements were performed by an experimenter blinded to the treatment conditions.

2.10 | In vitro TLR stimulation

B cells were isolated from WT mouse spleens as described above and plated in 96-well plates at a density of 5×10^6 cells/ml in RPMI 1640 containing 5% FBS, 1% L-glutamine, 200 $\mu\text{g}/\text{ml}$ penicillin, 200 U/ml streptomycin (all from Corning). Cells were incubated overnight with one of four concentrations of LPS (1, 5, 10, 20 $\mu\text{g}/\text{ml}$), Pam3CSK4 (0.01, 0.05, 0.1, 0.2 $\mu\text{g}/\text{ml}$), flagellin (0.1, 0.5, 2, 10 $\mu\text{g}/\text{ml}$), MALP-2 (10, 50, 100, 200 ng/ml) (all from Novus Biologicals), recombinant mouse heat-shock protein 60 (HSP60) (0.5, 1, 5, 10 $\mu\text{g}/\text{ml}$) (Abcam), recombinant mouse high-mobility group protein B1 (HMGB1) (0.5, 2, 5, 20 $\mu\text{g}/\text{ml}$) (Biolegend), and low molecular weight hyaluronic acid (HA) (0.1, 0.2, 0.5, 1 mg/ml) (R&D Biosystems) (see Figure 7). Control cells were maintained in RPMI media without stimulation. Cells were then incubated with 5 $\mu\text{g}/\text{ml}$ brefeldin A (Biolegend) for 4 h at 37°C , washed and stained for flow cytometry as described above. All experiments were run at least twice and included at least two technical replicates.

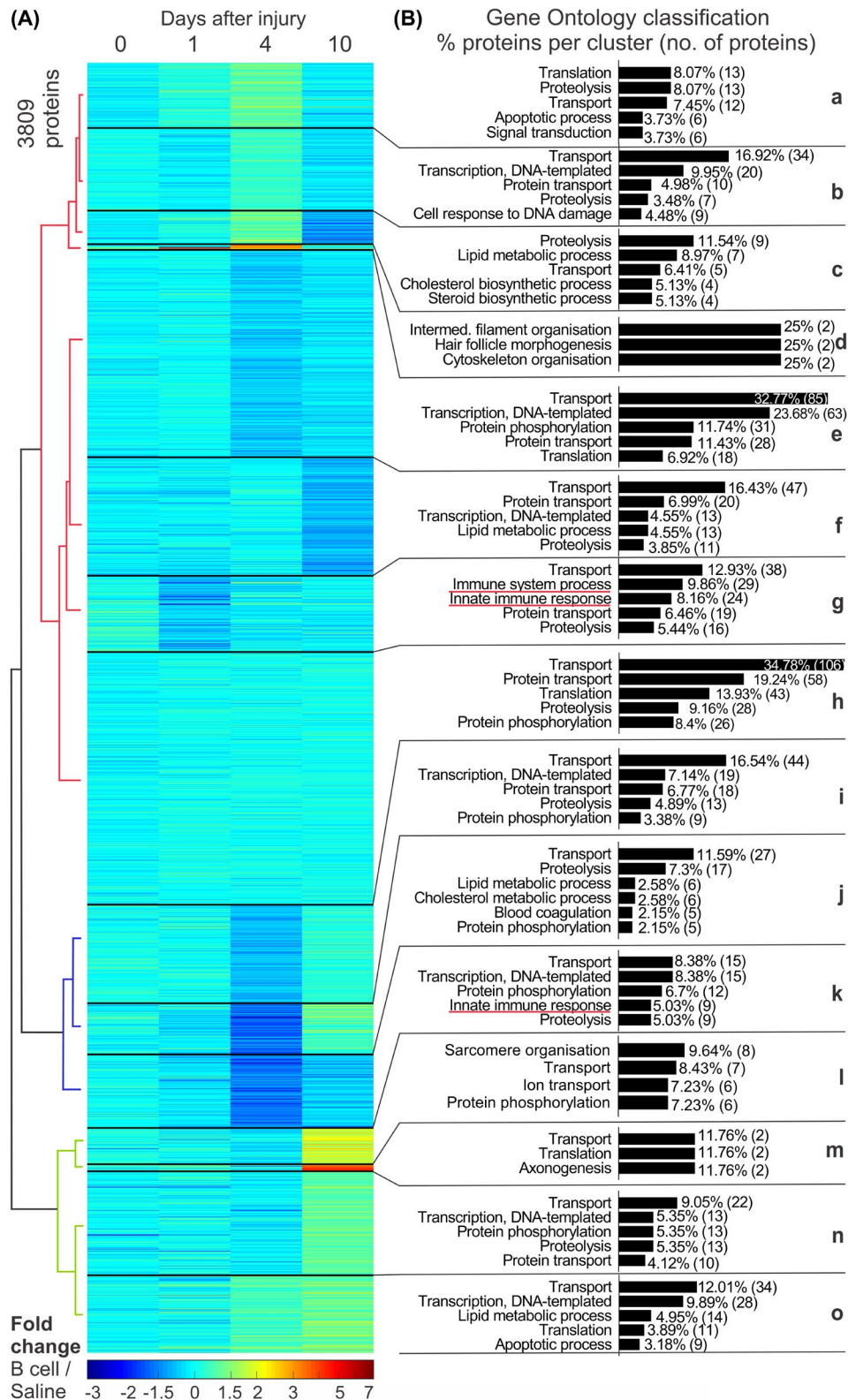
2.11 | Statistics

Sample sizes were determined based on previously published estimations for effect size and power for known paradigms (wound healing³ and TBI⁴) or otherwise determined as the minimal number of animals required for pairwise testing (exploratory investigations in tissue proteomics and single cell cytometric analysis). Statistical analyses were performed using GraphPad Prism 8 (GraphPad Software) or MATLAB (MathWorks). Prior to statistical testing, datasets were assessed for normal distribution using the D'Agostino & Pearson normality test. All reported descriptive statistics are estimated marginal means \pm standard error of the mean (SEM). p values $< .05$ were considered statistically significant.

3 | RESULTS

3.1 | Direct B cell application into injured tissue induces complex, time-dependent changes in the molecular microenvironment of the wound and accelerates molecular processes involved in healing

To examine the molecular changes that are associated with the direct introduction of purified B cells into an injured environment, we performed an exploratory proteomic analysis of whole wound biopsies at defined time



points during the process of wound healing. Multiplexed quantitative proteomics using tandem mass tag (TMT) reagents and MS3 quantification^{9,10,16} was performed on whole wound lysates identified a total of 9125 proteins across all samples and treatments. To allow direct

comparison between treatment conditions and across time points, only changes in abundance of proteins that were found in all samples ($n = 30$ animals, 3–5 animals/time point) were evaluated. This resulted in a total subset of 3809 proteins, which were hierarchically

FIGURE 1 B cell application induces complex changes in the injured microenvironment. (A) Proteomic analysis of wound tissue biopsies collected at 0 ($n = 4$ mice per treatment), 1 ($n = 4$ mice per treatment), 4 ($n = 5$ mice per treatment), or 10 ($n = 3$ mice per treatment) days after injury and treatment with either 1.5×10^6 wild-type B cells or saline control. Hierarchical clustering using Ward linkage was performed on the normalized, log-transformed fold change expression for the 3809 proteins (rows) consistently detected across all samples, treatments, and time points analyzed. The pseudocolor scale depicts values of the ratio between B cell-treated and saline-treated samples for each protein. The dendrogram shows 15 protein clusters derived from this analysis. Proteins cluster by their pattern of expression over all time points examined. (B) Gene ontology analysis of the 15 identified clusters was performed using the mouse GOSlim gene list from QuickGO (accessible at <https://www.ebi.ac.uk/QuickGO>). Bar graphs show the top 5 biological function categories for each cluster

clustered according to their pattern of expression over time (Figure 1A), resulting in 15 distinct clusters. B cell application was associated with changes in the expression of a large number of the analyzed proteins and included both up- and down-regulation as compared to saline-treated controls (Figure S1). As expected, some of the most pronounced changes in expression occurred at day 4 after injury, when the inflammatory and proliferative stages of wound healing overlap and create a highly dynamic microenvironment in the wound. Multiple clusters that showed down-regulation at this time point (Figure 1A—i,j,k) included proteins associated with proteolysis, lipid metabolism, and innate immune response among their top Gene Ontology (GO) categories (Figure 1B). Clusters that showed pronounced up-regulation in B cell-treated wounds included proteins associated with cytoskeleton organization and hair follicle morphogenesis (Figure 1A,B—d).

Upregulation was also observed at 10 days in clusters including proteins associated with sarcomere organization and axonogenesis (Figure 1A,B—l,m), suggesting on overall enhancement of specific regenerative processes in wounds that were treated with B cells at day 0. Interestingly, principal component analysis (PCA) performed on standardized protein abundances ($n = 38$ samples) also identified the most pronounced separation between B cell-treated wound samples and saline-treated controls at day 4. PCA separated groups of samples primarily by time point (i.e., healing stage). Notably, samples from day 4 wounds treated with B cells showed more similarity to samples collected from wounds at day 10 than to control saline-treated day 4 wounds (Figure 2). An in-depth analysis of the subset of proteins that were significantly changed relative to saline control at any given timepoint ($p < .05$, unpaired t -test) indicated that the largest proportion (42%) of these were associated with inflammatory cells or processes, and were mostly down-regulated, while the next largest category (12%) consisted of proteins associated with the regulation of oxidative stress (Figure 3) and showed elevated expression of protective factors. Together, these results indicate that application of B cells into the wound accelerates the molecular processes underlying wound healing, and that the largest

effect of B cell treatment is associated with modulating immune system-related protein expression.

3.2 | B cells applied directly into a wound respond in a time-dependent manner to molecular cues in the microenvironment and modulate the behavior of adjacent cells to promote tissue repair

Since global proteomic analysis indicated that B cell application can induce pleiotropic changes at specific time points during wound repair, we next assessed the time-dependent responses of the applied B cells, as well as adjacent immune cells and fibroblasts, using fluorescence flow cytometry. B cells or saline control were applied in vivo onto the wound bed or injected under uninjured skin in the same animal as a control for the effect of injury. After 18 h, 2, 4, or 10 days post-injury ($n = 3-6$ animals per time point and treatment), full-thickness biopsies were collected, dissociated and the cells in the wounds and subcutaneous injection sites were evaluated by flow cytometry for surface markers and levels of intracellular cytokines (Figure 4A,B). Approximately 20% of the exogenous B cells actively responded to the wound microenvironment with elevated production of multiple cytokines, as compared to the subcutaneous control condition. The B cell response was time-dependent, peaking at 2–4 days post-application for most cytokines, before decreasing after 4 days. Expression of the early activation marker CD69 was increased at 18 h after application, indicating a response to the change in microenvironment, independent of injury status. Significant increases were found at 2–4 days after application for regulatory cytokines, including IL-10, TGF β , and IL-4, as well as IL-2, IL-6, TNF α , and IFN γ (Figures 4C and S2), after which expression returned to baseline levels. One exception was the regulatory cytokine IL-10, which remained highly expressed in a significant proportion of B cells up to 10 days after application ($p < .05$). IL-35 showed a similar trend, although it did not reach significance. Interestingly, we found that the same subset of 20%–30% of the B cells that were applied to the

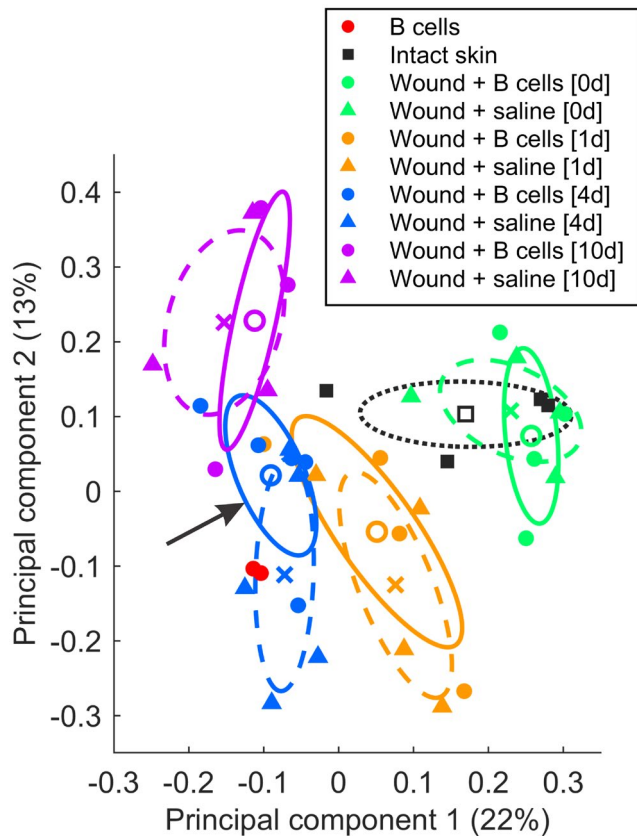


FIGURE 2 Principal components analysis of identified proteins shows wound healing progression. Principal components analysis was performed on standardized log-transformed abundances ($n = 38$ total samples) to uncover similarities in protein expression patterns across treatments and time points. For illustration, bivariate Gaussian distributions were fitted to the loading coefficients of the first two principal components, separately for each treatment group. The midpoints represent likelihood-weighted averages of the resulting distributions (open circles = B cell treatment; crosses = saline control), while the ellipses mark 50% probability contours for each sample group (continuous lines = B cell treatment; dashed lines = saline control). Note that at the 4-day timepoint the B cell treated sample distribution (*arrow*) localizes closer to the 10-day timepoint distributions, than to the saline control

wound environment responded by producing multiple immunomodulatory cytokines, instead of distinct B cell populations producing specific cytokines (Figure 4D). Control B cells that were maintained on ice for the matched time, preventing metabolic activity after isolation from the donor animals, indicate a very low baseline of cytokine production in the purified naïve cells, confirming that the cytokine response in B cells was associated with prolonged exposure to the wound microenvironment.

Because whole wound biopsies were dissociated for analysis, we were able to concurrently assess the responses of other infiltrating immune cells as well as fibroblast populations in each wound, in addition to B cells (Figure 4B).

In wounds that were treated with B cells as compared to saline control, at 4 days post-injury and treatment, significantly fewer infiltrating immune cells, comprising primarily neutrophils and macrophages (Figure S2), were positive for $\text{TNF}\alpha$ ($p < .001$). A trend towards a similar reduction associated with B cell treatment of the wound was observed for IL-2 and $\text{IFN}\gamma$ ($p < .1$). At the same 4-day time point, a significant increase in the proportion of leukocytes producing IL-35, IL-10, and $\text{TGF}\beta$ was measured (Figures 4A and S3B). The significant regulatory responses in these adjacent immune cell populations at 4 days after injury indicate a lag of 1–2 days after the peak B cell response to injury and is consistent with the results of the proteomic analysis. Using the same method, we also investigated the response of the wound and subcutaneous (non-injured control) fibroblasts when B cells or saline control were applied (Figure 5B). As expected, cellular activation and cytokine responses were more pronounced in fibroblasts located in the injured microenvironment as compared to uninjured subcutaneous control. Among the fibroblasts retrieved from the wound, a significant effect of B cell treatment was only observed for $\text{TNF}\alpha$, which was produced by a significantly lower number of fibroblasts in the B cell treated wounds at 4 days after injury, and conversely for $\text{TGF}\beta$, which remained expressed by up to 80% of the cells at 10 days after injury, while fibroblasts in the control wounds reduced their $\text{TGF}\beta$ expression to the baseline by this time point (Figures 5B and S3C). Together, these data suggest that the exogenous B cells respond to the wound microenvironment with a defined phenotypic shift, producing complex combinations of cytokines which subsequently modulate the responses of key cellular effectors of wound closure and tissue repair.

3.3 | MyD88-mediated TLR signaling is essential for the pro-regenerative and neuroprotective response of B cells after application in skin and brain injury, while IL-10 and IL-35 are key mediators of B cell function

To investigate the mechanisms that mediate B cell response after therapeutic application into an injured microenvironment, we set out to identify the essential molecules for B cell environmental sensing and the key molecular effectors that B cells use in order to modulate the immune responses in adjacent cells. In a full-thickness excision wound model, B cells purified from WT donors accelerated wound closure by 2–3 days relative to saline control, as previously described.³ In contrast, wounds treated with B cells from either $\text{MyD88}^{-/-}$ or $\text{IL-10}^{-/-}$ donors completely lost this regenerative benefit and closed at rates similar

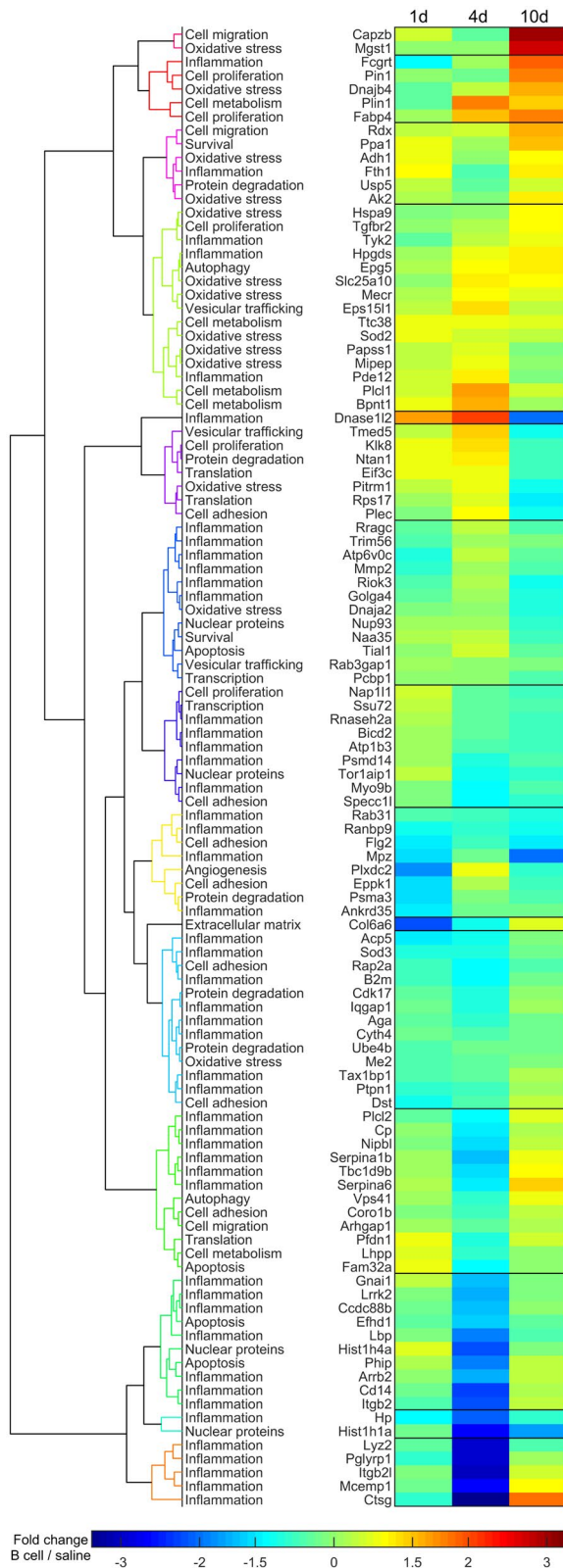


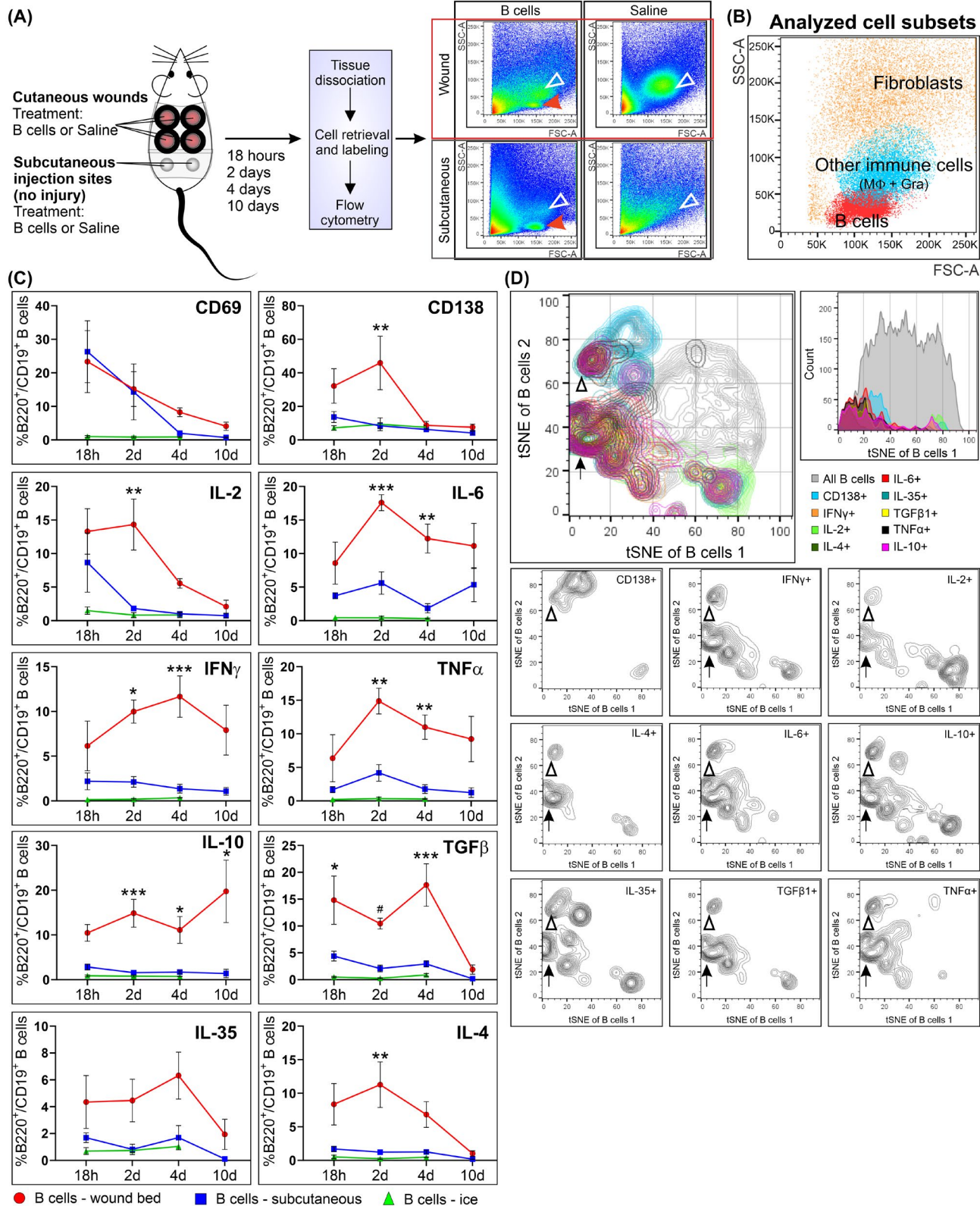
FIGURE 3 B cell application significantly regulates proteins associated with inflammation and repair in the context of wound healing. Heatmap of all proteins that showed differential expression between wounds treated with B cells and wounds treated with saline at any of the examined time points ($n = 108$). The pseudocolor scale depicts values of the ratio between B cell-treated and saline-treated samples for each protein. The dendrogram shows 15 protein clusters derived from this analysis. Clusters that showed pronounced down-regulation at 4 days post injury were enriched in proteins associated with inflammation and apoptosis. UniProt biological process categories relevant to wound healing were used for classification

from IL-35^{-/-} donors did prevent the initial inflammatory increase in wound size at day 2 post-injury, but ultimately did not significantly accelerate wound closure as compared to saline control. As a control for gene deficiency, we used B cells lacking TNF α , a pro-inflammatory cytokine that was not expected to affect the regenerative properties of B cells. Indeed, TNF α ^{-/-} B cells performed similarly to WT B cells, significantly accelerating wound closure as compared to saline control (Figure 6B). We have previously found that the application of WT B cells can also lead to improved quality of tissue repair, including a reduction in the size of the scar and improved collagen deposition, as well as enhanced angiogenesis.³ Histological analysis of healed wounds at 16 days post-injury showed that WT and TNF α ^{-/-} B cells induced a significant improvement in multiple parameters used to define the quality of regenerated tissue, including collagen deposition, patterning and maturation, width and thickness of the newly formed scar tissue, and angiogenesis (Figures 6C,D and S4).

By contrast, MyD88^{-/-}, IL-10^{-/-}, and IL-35^{-/-} B cells did not differ significantly from saline control on histological scores. We have shown previously³ that the treatment of wounds with WT B cells accelerates the egress of infiltrating neutrophils out of the wound bed approximately 2.5-fold as compared to control. To evaluate the impact of TLR-mediated signaling and anti-inflammatory cytokines on residual inflammation at 16 days post-injury, the presence of neutrophils in the scar tissue was quantified in tissue sections. Interestingly, the persistence of neutrophils at 16 days was overall inversely related to the healing score for each treatment category. Application of WT B cells was associated with a statistically significant reduction in the number of neutrophils only as compared to IL-10^{-/-} B cells or saline control, suggesting that IL-10 may play a key role in this aspect of B cell-mediated immunomodulation.

We next sought to confirm the role of MyD88 and IL-10 in the protective response of B cells in the context of a second injury model, namely a controlled cortical impact (CCI) paradigm of contusion TBI. We previously described functional and histopathological neuroprotective effects of mature naïve B cells applied directly to the site of CCI.⁴

to saline control (Figure 6A,B). B cells deficient in either MyD88 or IL-10 also did not prevent the initial enlargement of the open wound area at 2 days post-injury, associated with local edema and inflammation. The absence of IL-35, another key regulatory cytokine in B cells, also led to a significantly impaired pro-regenerative effect. B cells



Here, a similar set of behavioral paradigms (Figure S5A) were employed to determine whether the functional protection conferred by locally administered B cells is impaired by the absence of either MyD88 or IL-10. In the rotarod assay, intraparenchymal treatment with WT B lymphocytes had a significant protective effect (Figure 6F). Injured

mice treated with WT B cells performed similarly to their pre-injury baseline values, and consecutive trials showed a continued improvement in performance, suggesting that procedural learning occurred ($p < .0001$, time \times treatment interaction, two-way repeated measures ANOVA). By contrast, mice treated with MyD88^{-/-} or IL-10^{-/-} B cells, or

FIGURE 4 Purified B cells respond to a wound microenvironment through pleiotropic secretion of pro- and anti-inflammatory cytokines. (A) Experimental paradigm. Purified B cells were applied to full-thickness excision lesions or control subcutaneous sites. After exposure intervals of 18 h ($n = 6$ mice per group), 2 ($n = 6$ mice per group), 4 ($n = 6$ mice per group), or 10 days ($n = 3$ mice per group), the wounds were dissociated, and the whole cell suspension was labeled for flow cytometry analysis. A distinct lymphocyte population was detected in wounds treated with B cells (red arrowhead). In addition, other infiltrating immune cells, termed collectively non-B cell leukocytes for the purpose of the analysis, could be identified (open arrowhead). (B) Three main categories of cells were identified and evaluated in the dissociated wound or control site biopsies, including B cells, other immune cells comprising mostly infiltrating neutrophils and macrophages, and fibroblasts. (C) Time- and microenvironment-dependent response of experimentally applied B cells in vivo. Significantly higher percentages of the B cell population applied to the wound (red) as compared to subcutaneous control (blue) adopted a CD138⁺ plasma cell-like phenotype and produced both pro-inflammatory (IL-2, IL-6, IFN γ , TNF α) and anti-inflammatory (IL-4, IL-10, IL-35, TGF β) cytokines in a time-dependent manner, with the peak response observed at 2–4 days after application. The duration of the elevated cytokine production varied, with some cytokines such as IL-2 showing a very transient increase, while others, including IL-10, showing persistently elevated expression, up to day 10 after application. Control subsets of each batch of B cells maintained on ice (green) illustrate the negligible baseline production of each cytokine in the purified B cells. Data are shown as mean \pm SEM. Statistical analysis was performed using two-way ANOVA (treatment \times time point) followed by Sidak's multiple comparisons test, for each cytokine. # $p < .1$; * $p < .05$; ** $p < .01$; *** $p < .001$. (D) Representative example of t-distributed stochastic neighbor embedding plot of all B220⁺/CD19⁺ B cells illustrating subsets of the cell population that were gated as positive for each of the analyzed cytokines. Gating was performed using the same parameters as for the results shown in (C). The same subset of 20%–30% of the applied mature naïve B cells (arrows), including a subset of CD138⁺ plasma cells (open arrowheads), were found to express high levels of multiple pro- and anti-inflammatory cytokines in the wound environment, as shown by the overlap in the distributions of the gated populations. The example shown is the analysis of approximately 30,000 live B cells retrieved from a wound sample at 4 days after application

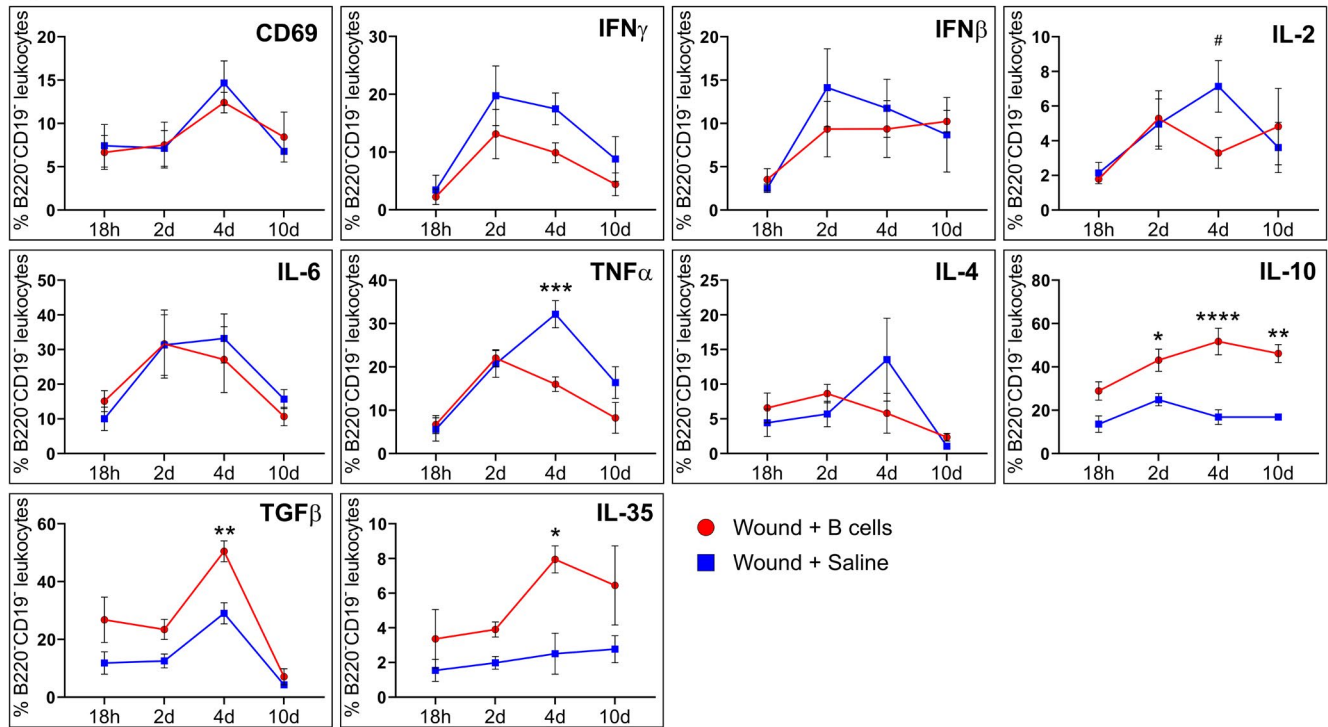
saline control performed significantly worse. Interestingly, IL-10^{-/-} B cells led to a somewhat milder phenotype than MyD88^{-/-} B cells or saline, suggesting a stronger impact of MyD88 deficiency (Figure 6F). In the MWM (Figure 6G–J), there was a significant overall effect of treatment ($p < .05$, two-way repeated measures ANOVA). Both WT and IL-10^{-/-} B cells were protective as compared to saline-treated controls in the hidden platform trials (Figure 6G), while MyD88^{-/-} B cells showed an intermediate effect ($p < .05$, Tukey's multiple comparisons test). No significant differences were observed in visible platform trials (Figure 6H). In probe trials assessing recall of spatial memory, WT B cell-treated mice were the only group that averaged above chance level (Figure 6I). Substantial effects of treatment were observed in the swim patterns of injured mice, with 80% of WT B cell treated mice demonstrating clearly directional spatial search strategies, whereas only 30% of saline-treated controls, 20% of the MyD88^{-/-} B cell-treated group and 0% of the IL-10^{-/-} B cell-treated group adopted spatial search strategies that would indicate cue awareness and learning (Figure 6J). In Y-maze testing, a working memory paradigm (Figure 6K), mice that received WT B cells intraparenchymally had alternation scores of 80 ± 1.3 SEM, significantly higher than animals treated with either MyD88^{-/-} B cells, IL-10^{-/-} B cells, or saline, suggesting improved memory of previously visited locations ($p < .0001$, one-way ANOVA). There was no significant difference between treatment groups with respect to the total number of maze arm entries ($p > .7$), indicating no group-associated differences in overall exploratory behavior. The NORT (Figure 6L) did not show significant differences, but similar trends as in the MWM were noted,

with WT and IL-10^{-/-} B cell treatments averaging above chance levels, while the MyD88^{-/-} B cell-treated and saline-treated groups were at or below chance level. As previously reported,⁴ no effect of treatment was observed in the elevated plus maze (Figure 6M), the wire grip test (Figure S5B), or the forced swim test (Figure S5C). The TBI lesion paradigm employed here is typically associated with a substantial degenerative cavitation at the injury site, which treatment with purified B cells was previously found to significantly reduce.⁴ To evaluate the impact of MyD88 and IL-10 on the ability of B cells to reduce structural injury, the total lesion volume at 100 days post-injury was determined. As in our previous studies, treatment with WT B cells led to an approximately 40% reduction in lesion volume as compared to saline control, while both MyD88^{-/-} B cells and IL-10^{-/-} B cells lost their neuroprotective effect and did not significantly reduce lesion size as compared to saline treatment (Figure 6N,O). Together, these results confirm that an intact MyD88-dependent TLR signaling pathway is required for the protective effects of B cells after CCI, and that IL-10 is one of the essential effector cytokines in this context.

3.4 | TLR 2, 4, and 6 mediate microenvironmental sensing by B cells placed in injured tissues by detecting endogenous damage-associated molecules

The essential role that MyD88 plays in enabling the pro-regenerative and neuroprotective effect of B cells indicates that microenvironmental sensing through surface TLRs

(A)



(B)

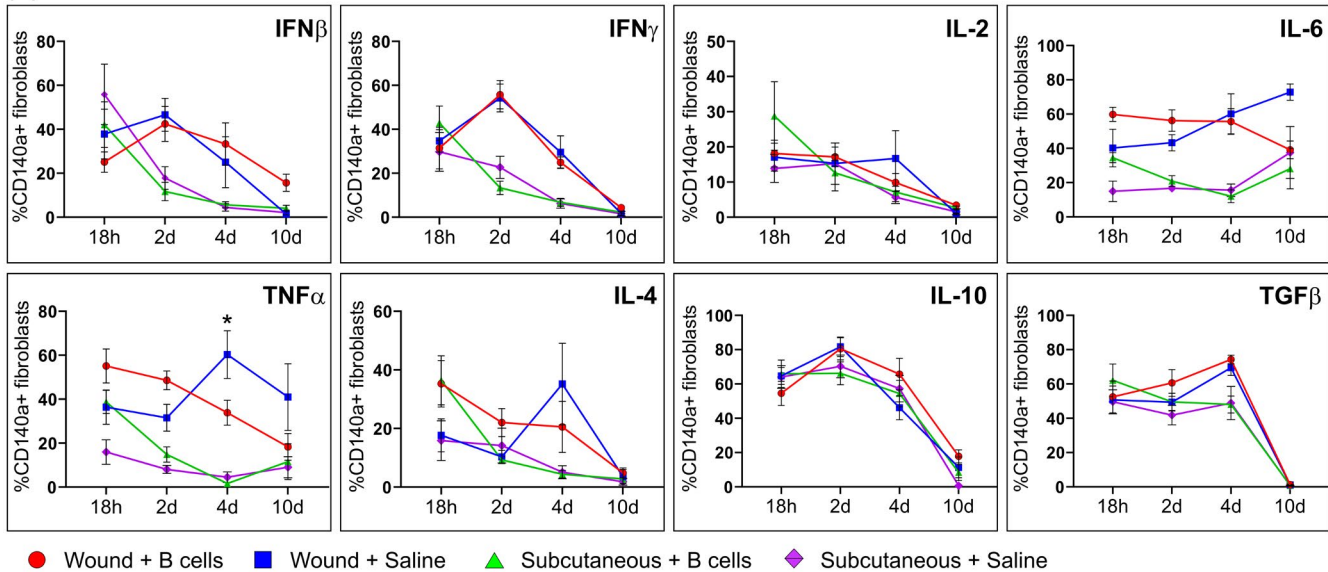


FIGURE 5 Experimentally applied B cells alter the dynamics of cytokine production in adjacent cells of the wound microenvironment. (A) Cytokine production over time was assessed in the aggregate population of non-B cell leukocytes, comprising primarily neutrophils (50%) and macrophages (16%), in wounds that were treated either with B cells (red) or saline control (blue). In the presence of B cells, a larger proportion of infiltrating leukocytes produced anti-inflammatory cytokines IL-10, transforming growth factor beta, and IL-35, and fewer produced pro-inflammatory tumor necrosis factor alpha (TNF α) and IL-2. This effect was most pronounced at 4 days after injury and treatment and persisted up to 10 days in the case of IL-10. (B) Dynamics of key cytokine expression in the CD140a⁺ fibroblast population of the wound and control subcutaneous tissue after treatment with B cells (red, wound; green, subcutaneous) or saline control (blue, wound; purple, subcutaneous). Overall, a significantly higher proportion of fibroblasts in the wound produced pro-inflammatory cytokines, including IFN β , IFN γ , IL-4, IL-6, and TNF α , as compared to the subcutaneous sites, regardless of wound treatment. Within the wound samples, B cell treatment was associated with a significant reduction in TNF α + fibroblasts at 4 days post-injury. Animal numbers and treatments as in Figure 4. Data are shown as mean \pm SEM. Statistical analysis was performed using two-way ANOVA (treatment \times time point) followed by Sidak's multiple comparisons test for each cytokine. # $p < .1$; * $p < .05$; ** $p < .01$; *** $p < .001$; **** $p < .0001$

is required for this response. To further explore which TLR pathways may be involved and which molecules in the extracellular environment may serve as relevant cues, purified mature naïve B cells were exposed to specific agonists for individual TLRs *in vitro*. B cells were stimulated with PAMPs, such as synthetic or bacterial-derived lipopeptides or lipopolysaccharides, including LPS (TLR4 agonist), Pam3CSK4 (TLR 1 and 2), flagellin (TLR 5), and MALP-2 (TLR 2 and 6), as well as DAMPs likely to be released from cells at the injury site, including HSP60 (TLR 2 and 4), HA (TLR4 agonist), and HMGB1 (TLR 2 and 4). Strong dose-dependent B cell activation, as indicated by increased CD69 expression, was induced by TLR 2, 4, and 6 agonists from both the DAMP and PAMP categories (Figure 7A). Response patterns resembling the pleiotropic cytokine production observed *in vivo* at 18 h were obtained after stimulation with LPS, Pam3CSK4, and MALP-2, suggesting the involvement of TLR 2, 4, and 6 in the microenvironment-sensing pathway in B cells. By contrast, TLR 5-specific stimulation with flagellin had minimal effect on the production of any of the measured cytokines. Among the DAMP stimuli, the nuclear protein HMGB1 and, to a lesser extent, the chaperone HSP60, induced the production of multiple cytokines. Interestingly, all the DAMP TLR agonists were also able to induce CD138 expression, resembling the plasma cell-like phenotype characteristic of B cell response *in vivo*, and suggesting that these proteins may represent some of the endogenous stimuli involved in the B cell activation observed in the wound. Supporting this observation, the pattern of expression for the assessed cytokines in B cells exposed to the wound environment *in vivo* for 18 h correlated significantly with the cytokine expression response of B cells stimulated for the same duration *in vitro* with HSP60 (Pearson $r = 0.9$, $p < .001$), HA (Pearson $r = 0.76$, $p < .05$), and HMGB1 (Pearson $r = 0.88$, $p < .001$), while PAMP TLR2/4 agonists yielded correlations under 0.5 that did not reach statistical significance. As observed *in vivo* (see Figure 4), B cells produced both pro- and anti-inflammatory cytokines in response to selective TLR activation, most notably IL-2, IFN γ , and TNF α , as well as IL-10, IL-35, and TGF β , respectively (Figure 7B).

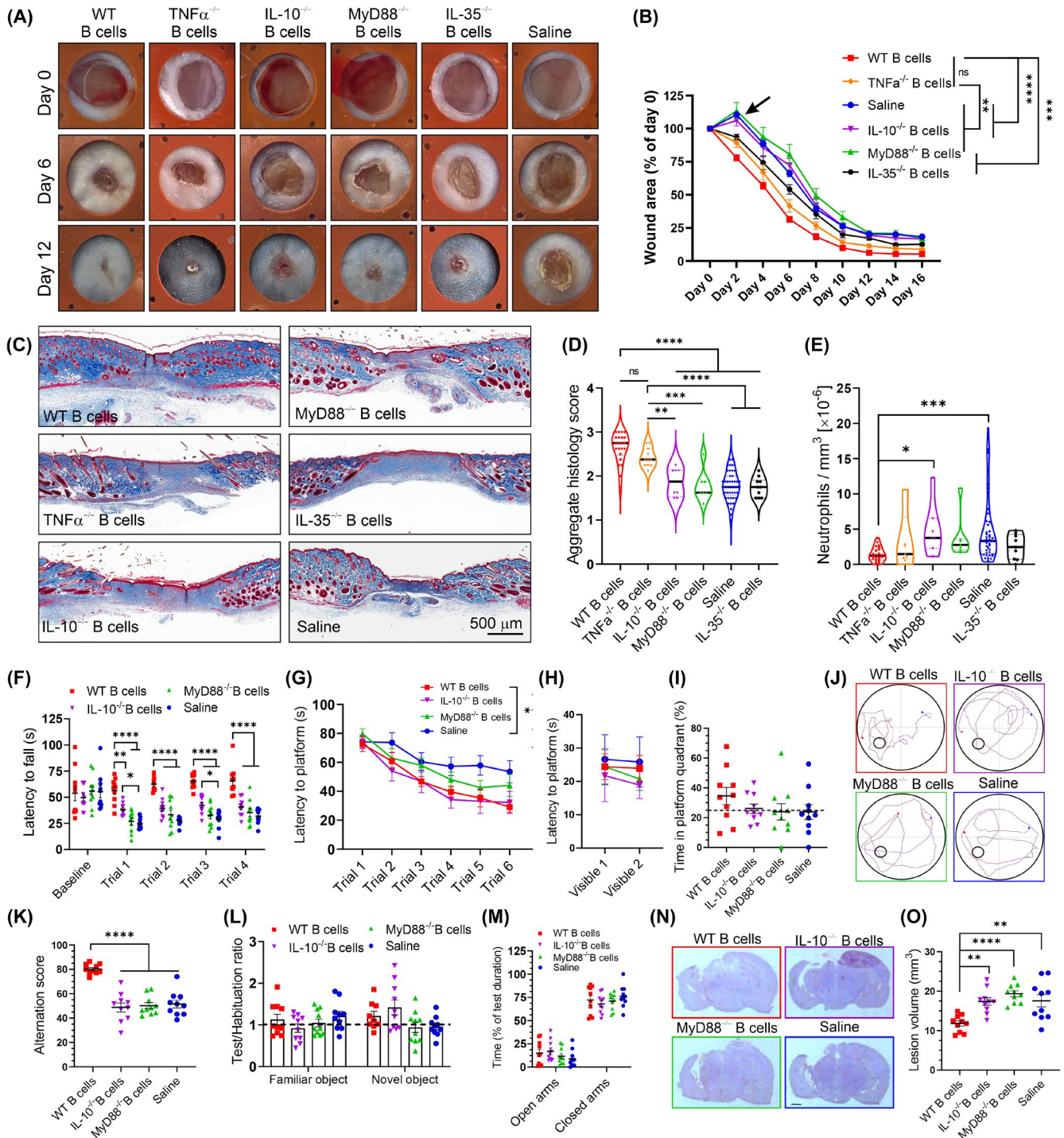
Although some variability in cytokine expression was observed between B cell subpopulations, the majority of both pro- and anti-inflammatory cytokines showed overlapping expression in the 4%–5% of the B cells that strongly responded to TLR stimulation. In summary, purified endogenous DAMPs that act through TLR 2/6 and TLR 4 pathways, particularly HSP60 and HMGB1, were able to induce a similar pleiotropic activation pattern in a subset of B cells as that observed *in vivo*, suggesting that this may be one of the mechanisms that induce B cell response after direct application into the wound microenvironment.

4 | DISCUSSION

4.1 | B cells applied directly into injured tissues can serve as complex immune regulators that promote repair by modulating the behavior of adjacent immune and stromal cells

Since the discovery of the immunoregulatory potential of B cells in the context of allergy and inflammation,¹⁷ numerous studies have confirmed the role of endogenous B cells as highly versatile immune regulators in models of autoimmunity, inflammation, and allergy.^{1,18} This potential has been harnessed in recent years to drive the development of therapeutic strategies in which exogenous B cells are used as disease-modifying cell-based therapeutics. B cells purified from bone marrow, spleen, or peripheral blood, have been shown by us and others to support repair in diverse models of tissue injury, including myocardial infarction,² stroke,^{5,6} acute and chronic cutaneous wounds,³ and contusion brain injury.⁴ The reproducibility of these findings across diverse experimental models suggests that common molecular mechanisms may underlie the reciprocal responses of B cells and the microenvironment of injured tissues.

This study provides a new perspective to our understanding of the way in which B cells act as therapeutic modulators of tissue repair. Our study describes the cellular and molecular mechanisms that accompany and mediate the direct introduction of B cells *in vivo*, in two distinct models of injury—cutaneous wound healing and TBI. In a model of wound healing, we show through two orthogonal methods—proteomic analysis and flow cytometry of whole-wound biopsy—that the activity of B cells alters the microenvironment and modulates the precise orchestration of the stages of tissue repair (Figure 8). Proteomic analysis revealed that B cells have a complex, time-dependent, homeostatic effect on the microenvironment of acute wounds, reducing the expression of proteins associated with inflammation, apoptosis, and oxidative stress, and increasing the expression of proteins associated with cell proliferation, cell growth, oxidative stress protection and control of inflammation, tissue growth, and remodeling. Of note, these effects were most pronounced 4 days after B cell treatment. PCA analysis showed that samples from B cell-treated wounds at day 4 are more similar overall to samples collected from wounds at day 10 than to paired control saline-treated day 4 wounds (Figure 2). This finding indicates a global shift in the molecular microenvironment of the wound, suggesting an accelerated timeline of healing. These results are in line with our earlier histological observations that B cell treatment significantly stimulates fibroblast proliferation and reduces apoptosis



within the granulation tissue of healing wounds at 4 days post injury, leading to overall faster wound closure and improved tissue remodeling compared to saline treated controls.³ At the same time points along the wound healing process, flow cytometry analysis of the infiltrating immune cells, including neutrophils and macrophages, as well as fibroblasts, reflected the aggregate results of the proteomic analysis with respect to an overall reduction in inflammation and up-regulation of pro-regenerative factors. In infiltrating immune cells, at 4 days after B cell application, there was a significant increase in anti-inflammatory and

pro-regenerative cytokines IL-10, IL-35, and TGF β , and a concomitant decrease in TNF α . TNF α is a marker of the early inflammatory phase in the context of wound healing and a decrease in TNF α synthesis is indicative of resolution of inflammation.¹⁹ Interestingly, TNF α in fibroblasts appears increased in B cell-treated wounds at early time points, before significantly decreasing as compared to saline-treated control by 4 days. This pattern may indicate an acceleration of the inflammatory stages of wound healing rather than a straightforward suppressive effect. In this context, we have previously described that the application

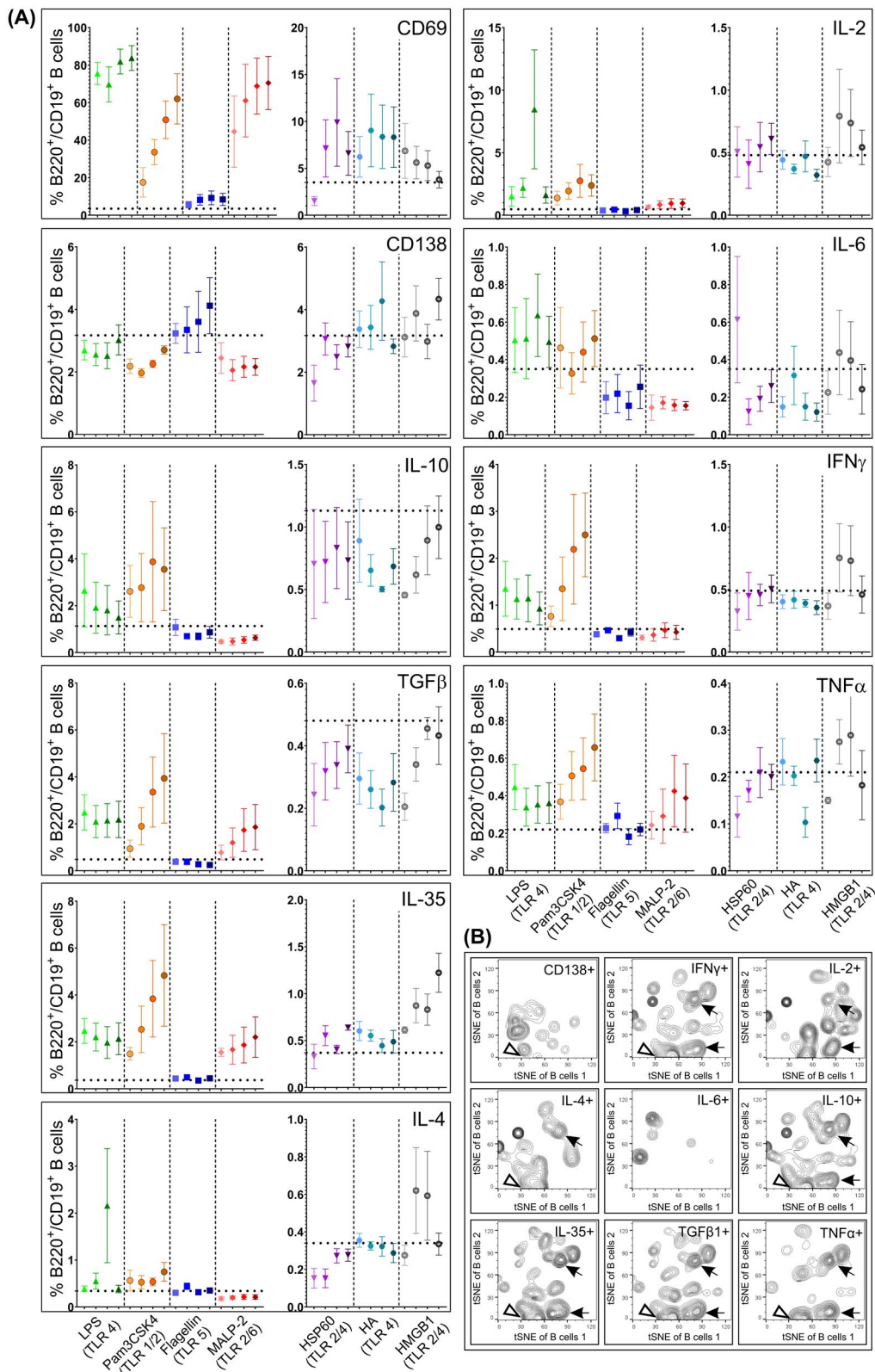
FIGURE 6 Functional toll-like receptor signaling as well as IL-10 production are necessary for the regenerative function of exogenous B cells in wound healing and their neuroprotective role in traumatic brain injury (TBI). (A–E) Wound healing model. (A) Full-thickness excision wounds (illustrated here at day 0, 6, and 12 of healing) were induced in the dorsal skin of wild-type (WT) mice, and treated at day 0 with 2×10^6 B cells purified from the spleen of WT C57Bl6, MyD88^{-/-}, IL-10^{-/-}, IL-35^{-/-}, or TNF α ^{-/-} isogenic animals, or saline control ($n = 10$ –45 per treatment). (B) Wounds were photographed every 2 days and the area of open wound was measured. For each wound, day 0 measurements were standardized as 100%, and values obtained on subsequent days were expressed as a percentage of the value at day 0. As described previously, WT B cells consistently accelerated the wound closure by 2–3 days. B cells from MyD88^{-/-} and IL-10^{-/-} donors did not accelerate wound closure, similar to saline controls, and even a small initial increase in wound area could be observed in these treatment categories at day 2, likely due to edema and inflammation (arrow). B cells from IL-35^{-/-} donors also performed significantly worse as compared to WT B cells, but did prevent the initial inflammatory response at day 2. B cells from TNF α ^{-/-} donors did not differ significantly from WT B cells in accelerating wound closure. Data are shown as mean \pm SEM. Statistical analysis was performed using two-way repeated-measures ANOVA (treatment \times time point), followed by Tukey's multiple comparisons test. (C) At day 16, biopsies from all wounds were collected, sectioned and stained for histological analysis using Masson's trichrome. (D) The quality of tissue repair was assessed via a composite score, comprising multiple measures of collagen deposition and orientation, the width of the scar and the thickness of the regenerated tissue, angiogenesis and cutaneous nerve regrowth. Data are shown as violin plots including all data points. Statistical analysis was performed using one-way ANOVA followed by Tukey's multiple comparisons test. (E) Residual infiltrating neutrophils at day 16 were quantified in tissue sections stained with H&E. Data are shown as truncated violin plots including all data points. Statistical analysis was performed using Kruskal-Wallis test, followed by Dunn's multiple comparisons test. (F–O) TBI model. C57Bl6 mice received a moderate-to-severe contusion TBI by controlled cortical impact and were treated at the time of injury with 2×10^6 B cells purified from the spleen of wild-type (WT) C57Bl6, MyD88^{-/-} or IL-10^{-/-} isogenic animals, or with saline control ($n = 10$ per treatment). Functional neuroprotection was assessed via a battery of behavioral tests, including rotarod (F), Morris water maze (G–J), Y maze (K), novel object recognition test (L), and elevated plus maze (M). Dashed lines in (I) and (L) indicate chance level. (N) At 100 days after TBI and treatment, the brains were collected, sectioned, and stained with hematoxylin for lesion volume analysis. (O) Quantification of residual brain lesion volume showed a significant neuroprotective effect of WT B cells that was abolished in MyD88^{-/-} or IL-10^{-/-} isogenic B cells. Data are presented as mean \pm SEM, with all points shown where feasible. Statistical analysis was performed using two-way repeated-measures ANOVA (treatment \times time point) (F, G, H, M) or one-way ANOVA (I, K, O), followed by Tukey's multiple comparisons test. ns, not significant; * $p < .05$; ** $p < .01$; *** $p < .001$; **** $p < .0001$

of B cells after cutaneous injury surprisingly led to higher infiltration of neutrophils into the wound bed but was then accompanied by accelerated clearance of neutrophils from the healing tissue.³ These benefits are likely maintained over long intervals, since in a contusion TBI model, B cells were found to reduce the numbers of activated CD68⁺ microglia and reactive astrocytes 35 days after application.⁴ In summary, our results consistently show that B cells applied at an injury site may contribute to local repair by exerting a multifactorial modulatory effect on multiple categories of adjacent immune and stromal cells.

4.2 | A heterogeneous population of B cells responds to the injury microenvironment with a complex and coordinated cytokine signature

It has been repeatedly found that a wide variety of B cells across developmental stages, ranging from early transitional B cells²⁰ to differentiated plasma cells,²¹ can adopt a regulatory phenotype upon appropriate stimulation. This indicates that this capacity is not a characteristic of a specialized B cell subpopulation, but rather a potential state of the majority of B cells.¹ To fully capture this diversity, in the present study, we applied a mix of purified splenic B cells into injured tissues, rather than

a pre-selected subpopulation. This mix included primarily B220⁺/CD19⁺/IgM⁺/IgD⁺ mature naïve B cells, with small subsets of CD22^{hi}/CD23^{lo} marginal zone B cells and CD23^{lo}/CD24^{hi} transitional B cells, and approximately 5% of spleen-resident B220^{lo}/IgD⁻/CD138⁺ plasmablasts and plasma cells.³ Three key findings in the present study are (i) that splenic purified B cells do not constitutively express significant levels of immunomodulatory cytokines, but rather initiate this response after at least 18 h in situ; (ii) that a relatively large proportion of up to 25% of the heterogeneous B cell mix applied to the wound microenvironment shows a synchronous multi-cytokine response; and (iii) that the response of exogenously applied B cells in the context of injury does not exclusively involve classical anti-inflammatory cytokines, such as IL-10 and IL-35, but also a series of factors canonically associated with inflammation, including IL-6 and TNF α . The B cell response in vivo also includes an up-regulation of CD138 expression, resembling a plasma cell-like phenotype, and the pleiotropic cytokine response signature was reproduced in this subset of cells (Figure 4D). However, it is important to note that the B cells applied in situ were never observed to proliferate in either the wound or the TBI model^{3,4} and thus the observed CD138⁺ phenotype likely does not correspond to a classical plasmablast/plasma cell profile.¹⁸ Moreover, a substantial subset of the retrieved B cells did not express any of the markers or cytokines evaluated



here, suggesting that the B cell response to injury may be selective and that there may be additional, yet uncharacterized, mechanisms of response in these cells.

The elevated production of IL-10, IL-35, and TGF β in a large proportion of B cells has well-documented regulatory effects on adjacent immune cells,^{22,23} and these

cytokines likely represent major molecular effectors that mediate the pro-regenerative and neuroprotective effect of B cells in injured skin and brain tissue, respectively. Indeed, IL-10 and IL-35 deletion severely impacted the protective ability of B cells in the wound healing model and partially in the TBI model. Interestingly, the same B

FIGURE 7 TLR2, TLR4, and TLR6 are candidate receptors that mediate the B cell response to the injured microenvironment. (A) To assess whether stimulation of individual toll-like receptor (TLR) pathways may induce a similar response of B cells *in vitro* as the cytokine profile observed *in vivo* in the context of wound healing, purified B cells were stimulated overnight with specific surface TLR agonists (LPS—TLR4; Pam3CSK4—TLR 1 and 2; Flagellin—TLR 5; MALP-2—TLR 2 and 6) or cell damage-associated proteins known to bind one or more TLRs (HSP60—TLR 2 and 4; low molecular weight HA—TLR 4; and HMGB1—TLR 2 and 4). In each condition, color intensity indicates increasing agonist concentrations. Horizontal dotted lines in each graph indicate the average response of B cells maintained in culture without any stimulation (control). Data are presented as mean \pm SEM. $n = 3$ independent experiments; all samples were processed in duplicate for each experiment. (B) Representative example of t-distributed stochastic neighbor embedding plot of all B220⁺/CD19⁺ B cells illustrating subsets of the cell population that were gated as positive for each of the analyzed cytokines. This analysis showed that after TLR-specific stimulation, similarly to the B cell response after *in vivo* exposure to the wound microenvironment, there was considerable overlap between the subsets of B cells that expressed high levels of multiple pro- and anti-inflammatory cytokines, as shown by the overlap in the distributions of the gated populations (arrows). A CD138⁺ plasma cell subset expressing mostly anti-inflammatory cytokines, also expressed IFN γ and TNF α (open arrowhead). The example shown is the analysis of approximately 26,000 B cells after stimulation with 1 μ g/ml LPS overnight

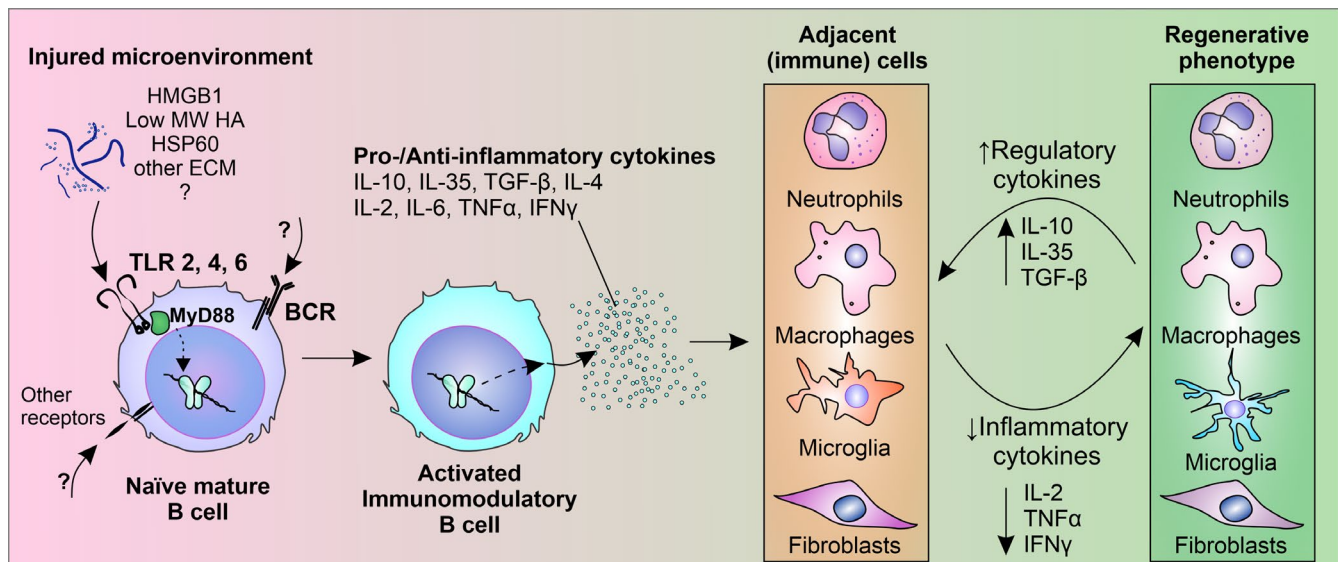


FIGURE 8 B cells applied exogenously into injured tissue microenvironments undergo a regulatory phenotypic shift, altering the response of adjacent resident and infiltrating immune cells to initiate a regenerative cellular and molecular cascade. Damage-associated molecular patterns from the injured environment stimulate mature, naïve B cells applied locally, via critical MyD88-dependent toll-like receptor sensing pathways, and potentially through secondary cellular sensing pathways. Activated B cells up-regulate the expression of CD138 and secrete multiple pro- and anti-inflammatory cytokines in a time-dependent manner. These B cell-derived immunomodulatory cytokines alter the infiltration/egress dynamics and the regulatory/inflammatory cytokine production of surrounding immune cells and immune-competent stromal cells, such as fibroblasts. Ultimately, this modulatory cascade leads to a local microenvironment that promotes regenerative processes and moderates the detrimental impact of excessive inflammation

cells that expressed high levels of regulatory cytokines also co-expressed high levels of IL-6, TNF α , IFN γ and to a lesser extent, IL-2 and IL-4, both *in vivo* and *in vitro*. These factors are typically associated with an inflammatory response; however, they also play important roles in regulating adjacent immune cells in injured tissues and orchestrating the initial stages of wound healing. For example, IFN γ has long been known to act as a regulator and chemotactic agent for neutrophils, activating and recruiting them to a site of inflammation; IFN γ binding leads to rapid internalization of receptors on the surface of neutrophils, ensuring the resolution of inflammation.²⁴

Interestingly, during an inflammatory response, neutrophils have been shown to induce the conversion of B cells into plasma cells by secreting B-cell activating factor (BAFF).²⁵ These modulatory interactions may underlie previous observations that B cell treatment leads to rapid infiltration of neutrophils into the wound bed, followed by accelerated clearance,³ and the finding in the current study that after application into the wound bed, B cells undergo a significant shift towards CD138⁺ plasma cell-like phenotype, particularly at 18–48 h after injury, when neutrophils are most abundant in the wound (Figure 4C). Further studies will be required to explore the regulatory

interplay between B cells and granulocytes in the context of tissue injury.

4.3 | MyD88-dependent TLR pathways mediate B cell response to injury

TLR activation is classically associated with pro-inflammatory responses to pathogen-associated molecular patterns, but also to injured and dying cells through damage-associated molecular patterns.²⁶ We hypothesized that TLR-mediated pathways are likely to play a key role in the ability of exogenously applied B cells to detect endogenous ligands released during cellular disruption or extracellular matrix degradation.^{26,27} In the context of tissue injury, it has been previously reported that extracellular matrix (ECM) components can induce CD19-dependent TLR signaling in the endogenous B cells localized in the wound, which in turn induces the expression of key cytokines such as IL-6, IL-10, and TGF- β .²⁸ In the present study, we found that deletion of MyD88, a key adaptor molecule required for TLR signaling,²⁹ from the applied B cells abolished their regenerative or neuroprotective effect in vivo, in the wound and in the TBI model, respectively. Since all TLRs except TLR3 utilize the MyD88-dependent signaling pathway, albeit not exclusively,^{29,30} it is likely that the binding of one or more TLRs is required for the B cell activation and subsequent regulatory response. Supporting this point, an elegant study in a mouse model of infection with *Salmonella typhimurium* found that mice controlled the infection far better when MyD88 was selectively ablated from their B cells.³¹ The authors report that this was a consequence of the TLR-mediated activation which induced a regulatory phenotype in B cells, which then suppressed three separate arms of protective immunity: neutrophils, natural killer cells, and inflammatory T cells.³¹ Since in the present study the injury models used were sterile, it is likely that the TLR-mediated B cell response is driven by activation through DAMPs rather than PAMPs. The complex signature of pleiotropic cytokines produced by B cells in response to in vivo stimulation could also be reproduced by in vitro stimulation with specific TLR agonists. Endogenous activators of TLRs are diverse and include high mobility group box 1 (HMGB1), a nuclear chromatin protein released from damaged cells via TLR4,³² heat shock proteins via TLR2 and TLR4,³³ and low molecular weight hyaluronic acid via TLR4.²⁸ While TLR activation is typically associated with a pro-inflammatory response in immune cells,^{29,30} in the present study we observed in vitro as well as in vivo the coordinated production of pro- and anti-inflammatory cytokines in the same subset of activated cells. It is important to note that a caveat of in vitro stimulation in the current

study is that B cells were exposed to single agonists in each condition, for 18 h. In vivo results at 18 h post application indicate that while the exogenous B cells appear to initiate their response to the wound microenvironment by this time point, robust, statistically significant changes in the expression of most cytokines require longer exposure times of approximately 2 days. In addition to the TLR agonists tested here, additional endogenous factors are also known activators of TLR receptors, including self-mRNA released by necrotic cells,³⁴ mitochondrial DNA,³⁵ and in the CNS, α -synuclein released by neurons³⁶ and A β peptides derived from amyloid precursor protein.³⁷ Thus, in vivo, multiple TLR agonists available in the injured microenvironment likely act simultaneously on exogenous B cells, inducing a more complex response in a larger proportion of the applied cells.

4.4 | Pligodraxis—A novel response of B lymphocytes in the context of tissue injury

We describe a unique response of mature naïve B cells upon introduction into an injured microenvironment, characterized by a complex cytokine signature that can induce regulatory changes in adjacent immune and stromal cells, and ultimately have a net positive impact on tissue repair. We term this novel phenomenon *pligodraxis*, from the Greek *pligí* = wound, and *drási* = action, indicating the specific activation of B cells in the microenvironment of injured tissues to drive an immunomodulatory and pro-regenerative response.

5 | SUMMARY

This study reveals for the first time the complex molecular pathways that underlie the capacity of mature naïve B cells to respond to and modulate the cellular microenvironment of injured tissues. These results reveal conserved time and stimulus-dependent dynamics of response in exogenous B cells, as well as novel cytokine signatures that open new possibilities of implementing targeted B cell-based therapies for the treatment of acute and chronic tissue injury. It will be important to investigate in further studies whether additional receptor and effector systems may be engaged in this context, and to elucidate the genetic switches that mediate the pleiotropic responses of exogenous B cells in situ.

ACKNOWLEDGEMENTS

This work was supported by funds from the NIH National Institute of Neurological Disorders and Stroke R01NS117598 to R.F.S., by Holy Cross Hospital, Ft.

Lauderdale, Florida, USA, to M.C.P., and the Vaccine and Immunotherapy Center Innovation Fund. This research was supported by the Specialized Histopathology Services Core Facility of the Dana-Farber/Harvard Cancer Center (P30 CA06516).

DISCLOSURES

The authors have no conflicting financial interests.

AUTHOR CONTRIBUTIONS

R.F.S. and M.C.P. designed the overall study. R.F.S. performed the experiments with assistance from A.M., C.S.Y.C., G.J., and D.S. M.B. performed data acquisition for proteomic analyses. I.I. performed statistical analysis of proteomic datasets. J.Y.C. performed the CCI paradigm. R.F.S., W.H., M.J.W., A.E.S., and M.C.P. designed experiments and drafted the manuscript.

DATA AVAILABILITY STATEMENT

All mass spectrometer RAW files can be accessed through the MassIVE data repository (massive.ucsd.edu) under the accession number MSV000086632.

ORCID

Ruxandra F. Sîrbulescu  <https://orcid.org/0000-0001-7905-1713>

REFERENCES

- van de Veen W, Stanic B, Wirz OF, Jansen K, Globinska A, Akdis M. Role of regulatory B cells in immune tolerance to allergens and beyond. *J Allergy Clin Immunol*. 2016;138:654-665.
- Goodchild TT, Robinson KA, Pang W, et al. Bone marrow-derived B cells preserve ventricular function after acute myocardial infarction. *JACC Cardiovasc Interv*. 2009;2:1005-1016.
- Sîrbulescu RF, Boehm CK, Soon E, et al. Mature B cells accelerate wound healing after acute and chronic diabetic skin lesions. *Wound Repair Regen*. 2017;25:774-791.
- Sîrbulescu RF, Chung JY, Edmiston W, Poznansky SA, Poznansky MC, Whalen MJ. Intraparenchymal application of mature B lymphocytes improves structural and functional outcome after contusion traumatic brain injury. *J Neurotrauma*. 2019;36:2579-2589.
- Bodhankar S, Chen Y, Vandembark AA, Murphy SJ, Offner H. IL-10-producing B-cells limit CNS inflammation and infarct volume in experimental stroke. *Metab Brain Dis*. 2013;28:375-386.
- Bodhankar S, Chen Y, Vandembark AA, Murphy SJ, Offner H. Treatment of experimental stroke with IL-10-producing B-cells reduces infarct size and peripheral and CNS inflammation in wild-type B-cell-sufficient mice. *Metab Brain Dis*. 2014;29:59-73.
- Kreuzer J, Edwards A, Haas W. Multiplexed quantitative phosphoproteomics of cell line and tissue samples. *Methods Enzymol*. 2019;626:41-65.
- Edwards A, Haas W. Multiplexed quantitative proteomics for high-throughput comprehensive proteome comparisons of human cell lines. *Methods Mol Biol*. 2016;1394:1-13.
- Ting L, Rad R, Gygi SP, Haas W. MS3 eliminates ratio distortion in isobaric multiplexed quantitative proteomics. *Nat Methods*. 2011;8:937-940.
- McAlister GC, Nusinow DP, Jedrychowski MP, et al. MultiNotch MS3 enables accurate, sensitive, and multiplexed detection of differential expression across cancer cell line proteomes. *Anal Chem*. 2014;86:7150-7158.
- Huttlin EL, Jedrychowski MP, Elias JE, et al. A tissue-specific atlas of mouse protein phosphorylation and expression. *Cell*. 2010;143:1174-1189.
- Eng JK, McCormack AL, Yates JR. An approach to correlate tandem mass spectral data of peptides with amino acid sequences in a protein database. *J Am Soc Mass Spectrom*. 1994;5:976-989.
- Elias JE, Gygi SP. Target-decoy search strategy for mass spectrometry-based proteomics. *Methods Mol Biol*. 2010;604:55-71.
- Bermpohl D, You Z, Lo EH, Kim HH, Whalen MJ. TNF alpha and Fas mediate tissue damage and functional outcome after traumatic brain injury in mice. *J Cereb Blood Flow Metab*. 2007;27:1806-1818.
- Mannix R, Meehan WP, Mandeville J, et al. Clinical correlates in an experimental model of repetitive mild brain injury. *Ann Neurol*. 2013;74:65-75.
- Lapek JD Jr, Greninger P, Morris R, et al. Detection of dysregulated protein-association networks by high-throughput proteomics predicts cancer vulnerabilities. *Nat Biotechnol*. 2017;35:983-989.
- Katz SI, Parker D, Turk JL. B-cell suppression of delayed hypersensitivity reactions. *Nature*. 1974;251:550-551.
- Fillatreau S. Regulatory plasma cells. *Curr Opin Pharmacol*. 2015;23:1-5.
- Ritsu M, Kawakami K, Kanno E, et al. Critical role of tumor necrosis factor- α in the early process of wound healing in skin. *J Dermatol Dermatol Surg*. 2017;21:14-19.
- Evans JG, Chavez-Rueda KA, Eddaoudi A, et al. Novel suppressive function of transitional 2 B cells in experimental arthritis. *J Immunol*. 2007;178:7868-7878.
- Shen P, Roch T, Lampropoulou V, et al. IL-35-producing B cells are critical regulators of immunity during autoimmune and infectious diseases. *Nature*. 2014;507:366-370.
- Iyer SS, Cheng G. Role of interleukin 10 transcriptional regulation in inflammation and autoimmune disease. *Crit Rev Immunol*. 2012;32:23-63.
- Rosser EC, Mauri C. Regulatory B cells: origin, phenotype, and function. *Immunity*. 2015;42:607-612.
- Ellis TN, Beaman BL. Interferon-gamma activation of polymorphonuclear neutrophil function. *Immunology*. 2004;112:2-12.
- Parsa R, Lund H, Georgoudaki AM, et al. BAFF-secreting neutrophils drive plasma cell responses during emergency granulopoiesis. *J Exp Med*. 2016;213:1537-1553.
- Kumar V. Toll-like receptors in the pathogenesis of neuroinflammation. *J Neuroimmunol*. 2019;332:16-30.
- Cambi A, Figdor C. Necrosis: C-type lectins sense cell death. *Curr Biol*. 2009;19:R375-R378.
- Iwata Y, Yoshizaki A, Komura K, et al. CD19, a response regulator of B lymphocytes, regulates wound healing through hyaluronan-induced TLR4 signaling. *Am J Pathol*. 2009;175:649-660.
- Kawai T, Akira S. Toll-like receptors and their crosstalk with other innate receptors in infection and immunity. *Immunity*. 2011;34:637-650.

30. Li L, Acioglu C, Heary RF, Elkabes S. Role of astroglial toll-like receptors (TLRs) in central nervous system infections, injury and neurodegenerative diseases. *Brain Behav Immun*. 2021;91:740-755.
31. Neves P, Lampropoulou V, Calderon-Gomez E, et al. Signaling via the MyD88 adaptor protein in B cells suppresses protective immunity during *Salmonella typhimurium* infection. *Immunity*. 2010;33:777-790.
32. Sun L, Li M, Ma X, et al. Inhibition of HMGB1 reduces rat spinal cord astrocytic swelling and AQP4 expression after oxygen-glucose deprivation and reoxygenation via TLR4 and NF-kappaB signaling in an IL-6-dependent manner. *J Neuroinflammation*. 2017;14:231.
33. Asea A, Rehli M, Kabingu E, et al. Novel signal transduction pathway utilized by extracellular HSP70: role of toll-like receptor (TLR) 2 and TLR4. *J Biol Chem*. 2002;277:15028-15034.
34. Kariko K, Ni H, Capodici J, Lamphier M, Weissman D. mRNA is an endogenous ligand for toll-like receptor 3. *J Biol Chem*. 2004;279:12542-12550.
35. Bao W, Xia H, Liang Y, et al. Toll-like receptor 9 can be activated by endogenous mitochondrial DNA to induce podocyte apoptosis. *Sci Rep*. 2016;6:22579.
36. Fellner L, Irschick R, Schanda K, et al. Toll-like receptor 4 is required for alpha-synuclein dependent activation of microglia and astroglia. *Glia*. 2013;61:349-360.
37. Liu S, Liu Y, Hao W, et al. TLR2 is a primary receptor for Alzheimer's amyloid beta peptide to trigger neuroinflammatory activation. *J Immunol*. 2012;188:1098-1107.

SUPPORTING INFORMATION

Additional supporting information may be found in the online version of the article at the publisher's website.

How to cite this article: Șirbulescu RF, Mamidi A, Chan S-YC, et al. B cells support the repair of injured tissues by adopting MyD88-dependent regulatory functions and phenotype. *FASEB J*. 2021;35:e22019. doi:[10.1096/fj.202101095RR](https://doi.org/10.1096/fj.202101095RR)